Pure dephasing of single Mn spin in semiconductor quantum dots

Dingyang Liu, Wenxi Lai, and Wen Yang*
Beijing Computational Science Research Center, Beijing 100193, China
(Received 19 July 2016; revised manuscript received 4 July 2017; published 30 August 2017)

We present comprehensive analytical and numerical studies on the pure dephasing of a single Mn spin in a semiconductor quantum dot due to (i) its *sp-d* exchange interaction with an electronic environment, and (ii) its hyperfine interaction with the nuclear spin environment. For (i), by modeling the electronic environment by an open two-level system, we provide exact analytical expressions and present detailed analysis for the Mn spin pure dephasing in both the Markovian and non-Markovian regimes. This provides a clear physical picture and a general theoretical framework based on which we estimate the Mn spin pure dephasing due to various fluctuations (such as thermal excitation, optical pumping, tunneling, or electron/hole spin relaxation) of the electronic environment and reveals a series of interesting behaviors, such as thermal, optical, and electrical control of the crossover between the Markov and non-Markov regimes. In particular, we find rapid Mn spin pure dephasing on a nanosecond time scale by the thermal fluctuation and optical pumping, but these mechanisms can be strongly suppressed by shifting the electron envelope function relative to the Mn atom with an external electric field through the quantum-confined Stark effect. The thermal fluctuation mechanism is also exponentially suppressed at low temperature. For (ii), we find that the Mn spin dephasing time is limited by the thermal fluctuation of the nuclear spins to a few microseconds even at low temperature and its value varies from sample to sample, depending on the distribution of spinful isotopes on the nearest-neighbor sites surrounding the substitutional Mn atom. Our findings may be useful to understand and suppress the Mn spin pure dephasing for its applications in quantum information processing.

DOI: 10.1103/PhysRevB.96.075443

I. INTRODUCTION

With the constant progress in the precise control of semiconductor doping, a new field of solotronics is opening up [1–4], which utilizes individual dopant ions and defects in semiconductors for applications in various quantum technologies such as quantum computation, sensing, communication, and on-demand photon sources. A promising candidate that allows for electrically controlled operation is a single magnetic ion embedded in a semiconductor quantum dot (QD). In particular, the transition-metal Mn ion has a half-filled $3d^5$ electronic configuration and acts as a completely localized large spin $S = 5/2$, which is coupled to the spin of the band carriers via *sp-d* exchange interaction [5]. In recent years, there have been extensive theoretical studies on the electro-optical [6–13] and magnetic [14–19] properties as well as electron spin relaxation [20] in Mn-doped QDs. Experimentally, the *sp-d* exchange interaction between the Mn spin and the electron/hole spin leads to the splitting of an exciton line in the photoluminescence spectrum of the QD [21–28] and allows observing dark-exciton transitions [29]. Moreover, the *sp-d* exchange interaction enables controlling the Mn spin by injecting spin-polarized carriers via electrical gating or optical pumping [27,30,31]. Recently, remarkable success has been achieved in the initialization, manipulation, and readout of the Mn spin in individual QDs [22,28,31–38].

A main obstacle to the practical applications of a localized spin in individual QDs is the decoherence caused by environmental noises [39–41]. The spin decoherence include two processes: (1) relaxation of its populations on the Zeeman energy sublevels, i.e., the *spin relaxation* or T_1 process; (2) randomization of the relative phase between different Zeeman eigenstates of the superposition, i.e., the *pure dephasing* or T_φ process (see Ref. [42] for a pedagogical introduction). For Markovian environments, the total dephasing is the sum of pure dephasing and the dephasing due to relaxation, i.e., $1/T_2 = 1/T_\varphi + 1/(2T_1)$ (Ref. [42]). For paradigmatic solid-state spin qubits, such as electron spins in semiconductor QDs, phosphorus and bismuth donors in silicon, and nitrogen-vacancy centers in diamond, the pure dephasing time $T_\varphi \ll T_1$, so that $T_2 \approx T_\varphi$. In other words, it is the pure dephasing, instead of the spin relaxation, that sets the ultimate limitation to their applications to quantum technologies. This observation highlights the importance of understanding and suppressing the pure dephasing of a single Mn spin in QDs.

In the past few years, many experimental and theoretical works provided valuable information on the spin relaxation of a single Mn spin in QDs; e.g., an isolated Mn spin has T_1 ranging from a few microseconds up to 0.1 ms (Refs. [36,43–45]), but it decreases to the nanosecond time scale in the presence of band carriers [4,33–36,44,46,47]. For a diluted ensemble of Mn spins in the MgO crystal, the Rabi oscillation decay time $\sim$0.5 μs is limited by the hyperfine interaction with the ^{25}Mg nuclear spin bath [48]. For an ensemble of Mn spins in polar piezoelectric ZnO QDs, their dephasing time is limited to $T_2 \approx T_\varphi \approx 0.8$ ms by the interactions between neighboring Mn spins at low temperature [49]. However, very little is known about the T_φ of a single Mn spin in individual QDs. The recent experiment by Goryca *et al.* [38] only gives a lower bound $T_2 \approx T_\varphi \geqslant 1.8$ ns that is several orders of magnitudes shorter than the Mn spin relaxation time $T_1 \sim 0.1$ ms. In this context, it is highly desirable to develop a clear physical picture and a realistic estimate for the Mn spin pure dephasing, especially in the presence of carriers (electrons and/or holes). Up to date, however, we are not aware of any further experimental or theoretical study along this direction.

*wenyang@csrc.ac.cn

In this paper, we perform both analytical and numerical studies on the *pure dephasing* of a single Mn spin $S = 5/2$ in a QD due to magnetic noises from two important environments: (i) the electronic environment, which is coupled to the Mn spin through the *sp-d* exchange interaction; (ii) the surrounding nuclear spins, which are coupled to the Mn spin through the hyperfine interaction. For case (i), the magnetic noise may come from the random hopping of the electrons and/or holes between different orbitals or the random flip of their spins. By modeling the electronic environment by an open two-level system, we provide exact analytical solutions and detailed physical analysis for the Mn spin pure dephasing in both the Markovian and non-Markovian regimes, which agree with our numerical simulations and exhibit a series of interesting behaviors, such as the thermal and optical control of the Mn spin pure dephasing rate and the crossover from the Markovian regime into the non-Markovian regime, accompanied by the appearance of pronounced modulations in the dephasing profile. This establishes a clear physical picture and a general theoretical framework based on which we estimate the Mn spin pure dephasing due to various fluctuations of the electronic environment, such as thermal excitation, optical pumping, electron/hole tunneling into and out of the QD, and electron/hole spin relaxation, relevant to a wide range of experiments [22,28,31–38]. In particular, we find the thermal fluctuation of the electron and/or hole and optical pumping lead to Mn spin pure dephasing on the nanosecond time scale, but they can be strongly suppressed by several orders of magnitude by shifting the electron/hole envelope function relative to the Mn atom with an external electric field through the quantum-confined Stark effect. The thermal fluctuation mechanism is also strongly suppressed at low temperature. For case (ii), the Mn spin pure dephasing time is typically limited by the nuclear spin thermal fluctuation to a few microseconds, consistent with the previous experimental measurement [48]. Our findings may be useful to understanding and prolonging the Mn spin dephasing time for its applications in quantum technologies.

This paper is organized as follows. In Sec. II, we first introduce the commonly used Markov approximation and then model the electronic environment by an open two-level system and provide exact analytical solutions and detailed physical analysis for the Mn spin dephasing rate and dephasing profile in the Markovian and non-Markovian regimes. In Sec. III, we apply these analytical formulas together with numerical simulation to study electron-induced Mn spin dephasing due to thermal excitation and optical pumping and further demonstrate the suppression of these mechanisms by applying an electric field. We also briefly discuss Mn spin pure dephasing by other fluctuation mechanisms, including thermal excitation of the heavy hole, tunneling of carriers into and out of the QD, and spin relaxation of the electron or the hole. In Sec. IV, we study the Mn spin pure dephasing by the nuclear spin environment. Finally, a brief conclusion is given in Sec. V. For brevity, we set $\hbar = 1$ throughout this work.

II. PHYSICAL PICTURE OF Mn SPIN DEPHASING

We consider a single Mn spin-5/2 located at $\mathbf{R}$ under an external magnetic field along the z axis. The Hamiltonian of the Mn spin is $\omega_M \hat{M}_z$, where $\omega_M \equiv g_M \mu_B B$ is the Zeeman splitting and g_M is the Landé factor of the Mn spin. The coupling of the Mn spin and the environment can be written as $\hat{\mathbf{M}} \cdot \hat{\mathbf{h}}$, where $\hat{\mathbf{h}}$ is an operator of the environment. For example, the *s-d* exchange interaction between the Mn spin $\hat{\mathbf{M}}$ and the electron spin $\hat{\mathbf{S}}_e$ corresponds to

$$\hat{\mathbf{h}} = -J_e \hat{\mathbf{S}}_e \delta(\hat{\mathbf{r}}_e - \mathbf{R}), \tag{1}$$

being proportional to the electron spin density at the location of the Mn atom, where $\hat{\mathbf{r}}_e$ is the electron position operator and J_e is the *s-d* exchange constant. The *p-d* exchange interaction [44,50] between the Mn spin $\hat{\mathbf{M}}$ and the *heavy*-hole spin $\hat{\mathbf{S}}_h$ corresponds to

$$\hat{\mathbf{h}} = -\frac{1}{3} J_h \hat{S}_{h,z} \mathbf{e}_z \delta(\hat{\mathbf{r}}_h - \mathbf{R}), \tag{2}$$

being proportional to the hole spin density at the location of the Mn atom, where $\hat{\mathbf{r}}_h$ is the hole position operator, J_h is the *p-d* exchange constant, and $\mathbf{e}_z$ is a unit vector along the z axis. The dipolar hyperfine interaction with a collection of surrounding nuclear spins $\{\hat{\mathbf{I}}_n\}$ located at $\{\mathbf{R}_n\}$ corresponds to [42]

$$\hat{\mathbf{h}} = \sum_n \frac{\mu_0}{4\pi\rho_n^3} \gamma_e \gamma_n \left(\hat{\mathbf{I}}_n - 3\frac{(\hat{\mathbf{I}}_n \cdot \boldsymbol{\rho}_n)\boldsymbol{\rho}_n}{\rho_n^2} \right), \tag{3}$$

where $\boldsymbol{\rho}_n \equiv \mathbf{R} - \mathbf{R}_n$, and $\gamma_e = -1.76 \times 10^{11}$ rad/(s T) and γ_n are, respectively, the gyromagnetic ratio of a free electron and the nth nuclear spin $\hat{\mathbf{I}}_n$. The total Hamiltonian of the Mn spin and the environment is the sum of the Mn spin Zeeman Hamiltonian $\omega_M \hat{M}_z$, its coupling to the environment $\hat{\mathbf{M}} \cdot \hat{\mathbf{h}}$, and the environment Hamiltonian $\hat{H}_E$.

The environment operator $\hat{\mathbf{h}}$ serves as an effective magnetic field on the Mn spin, in analogy to the Zeeman coupling of the Mn spin to an external magnetic field. However, $\hat{\mathbf{h}}$ differs from a deterministic magnetic field in that it undergoes random fluctuation. This point becomes clear in the interaction picture of the electronic environment, where the total Hamiltonian becomes $\omega_M \hat{M}_z + \hat{\mathbf{M}} \cdot \hat{\mathbf{h}}(t)$ and $\hat{\mathbf{h}}(t) \equiv e^{i\hat{H}_E t} \hat{\mathbf{h}} e^{-i\hat{H}_E t}$ can be regarded as the quantum analogy of the classical noise. Therefore, the interaction of the Mn spin with the environment generates a randomly fluctuating quantum noise $\hat{\mathbf{h}}(t)$ acting on the Mn spin. The mean-field part $\langle \hat{\mathbf{h}}(t) \rangle$ renormalizes the Mn spin Larmor frequency, while the fluctuation part $\delta\hat{\mathbf{h}}(t) \equiv \hat{\mathbf{h}}(t) - \langle \hat{\mathbf{h}}(t) \rangle$ leads to Mn spin decoherence: the transverse fluctuation $\delta\hat{h}_x(t)$ and $\delta\hat{h}_y(t)$ leads to Mn spin relaxation, while the longitudinal fluctuation $\delta\hat{h}_z(t)$ leads to Mn spin pure dephasing [42].

A. Born-Markov approximation

When $\delta\hat{\mathbf{h}}(t)$ fluctuates much faster than the Mn spin decoherence, the Born-Markov approximation can be employed to derive the master equation for the reduced density matrix $\hat{\rho}$ of the Mn spin [51,52]. When the Mn spin decoherence is much slower than its Larmor precession (with frequency $|\omega_M|$) and different Cartesian components of $\delta\hat{\mathbf{h}}(t)$ have no cross-correlation, i.e., $\langle \delta\hat{h}_\alpha(t) \delta\hat{h}_\beta \rangle \propto \delta_{\alpha,\beta}$, the master equation reads

$$\dot{\rho}(t) = -i[(\omega_M + \langle \hat{h}_z \rangle)\hat{M}_z, \hat{\rho}(t)] + \sum_{\alpha=z,\pm} \Gamma_\alpha \mathcal{D}[\hat{M}_\alpha]\hat{\rho}, \tag{4}$$

where $\mathcal{D}[\hat{L}]\hat{\rho} \equiv \hat{L}\hat{\rho}\hat{L}^\dagger - \{\hat{L}^\dagger\hat{L},\hat{\rho}\}/2$ describes the dissipation in the Lindblad form and

$$\Gamma_z = 2\,\mathrm{Re}\int_0^\infty \langle \delta\hat{h}_z(t)\delta\hat{h}_z\rangle dt, \tag{5}$$

$$\Gamma_\pm = 2\,\mathrm{Re}\int_0^\infty [\langle \delta\hat{h}_x(t)\delta\hat{h}_x\rangle + \langle \delta\hat{h}_y(t)\delta\hat{h}_y\rangle]e^{\mp i\omega_M t}dt. \tag{6}$$

In Eq. (4), the $\alpha = z$ term describes the Mn spin pure dephasing and the $\alpha = \pm$ terms describe the Mn spin relaxation. For a simple example, we assume $\delta\hat{h}_\alpha(t)$ has a characteristic fluctuation rate γ (or memory time $1/\gamma$) and autocorrelation $\langle \delta\hat{h}_\alpha(t)\delta\hat{h}_\alpha\rangle = \langle(\delta\hat{h}_\alpha)^2\rangle e^{-\gamma|t|}$. This gives

$$\Gamma_z = 2\pi\langle(\delta\hat{h}_z)^2\rangle\delta^{(\gamma)}(0),$$

$$\Gamma_\pm = 2\pi\langle(\delta\hat{h}_x)^2 + (\delta\hat{h}_y)^2\rangle\delta^{(\gamma)}(\omega_M),$$

where $\delta^{(\gamma)}(\Delta) \equiv (\gamma/\pi)/(\Delta^2+\gamma^2)$ is the Lorentzian shape function.

The expressions above show that the widely studied Mn spin relaxation differs significantly from the Mn spin pure dephasing—the focus of our present work—in that they originate from different frequency components of the noise. The former originates from noises that fluctuate at frequency ω_M, so it increases with increasing γ (until $\gamma > |\omega_M|$), while the latter originates from the zero-frequency component of the noise, so rapidly fluctuating noises lead to slow pure dephasing. This underlies the motional narrowing phenomenon in magnetic resonance spectroscopy [42,51], where the random motion of atoms makes the magnetic noise fluctuate faster and hence slows down the central spin decoherence (manifested as the narrowing of the linewidth of the magnetic resonance line of the central spin). Since the Mn spin relaxation has been studied extensively in previous works, here we neglect h_x, h_y and focus on pure dephasing. Taking the off-diagonal matrix elements of Eq. (4) in the Zeeman basis $\{|m\rangle\}$ (i.e., $\hat{M}_z|m\rangle = m|m\rangle$) of the Mn spin gives the off-diagonal coherence:

$$\frac{\rho_{mm'}(t)}{\rho_{mm'}(0)} = e^{-i(m-m')(\omega_M+\langle\hat{h}_z\rangle)t}e^{-\Gamma_z(m-m')^2t/2}, \tag{7}$$

which decays exponentially at a rate proportional to the square of the coherence order $|m-m'|$. The first-order coherence $\rho_{m,m\pm1}(t)$ exhibits the minimum decay rate $\Gamma_z/2$. Before going into specific physical mechanisms, we first establish a simple but general physical picture that allows us to understand and estimate the Mn spin pure dephasing in different experimental setups.

B. Two-level model: Exact solutions

For a single Mn spin in a semiconductor QD, the most relevant electronic environment could be a single extra electron, a single extra hole, a neutral exciton, a negatively charged exciton (two electrons and one hole), or a positively charged exciton (two holes and one electron). These environments have discretized energy levels and their fluctuation could be caused by thermal excitation (i.e., phonon scattering), electron/hole tunneling between the QD and an electron/hole reservoir near the QD, optical pumping, or relaxation of the electron/hole spin. To establish a simple physical picture, we regard the electronic environment as an *open* two-level system coupled to another Markovian bath. We assume the ground state $|g\rangle$ is lower than the excited state $|e\rangle$ by an energy ω_0 and characterize the bath-induced random hopping of the electronic environment by the transition rate γ_g from $|g\rangle$ to $|e\rangle$ and the transition rate γ_e from $|e\rangle$ to $|g\rangle$. This establishes the ground state population $P_g = \gamma_e/(\gamma_g+\gamma_e)$ and excited state population $P_e = 1 - P_g$ in the steady state, which could differ from a thermal equilibrium state when the electronic system is under external driving, such as optical pumping. The quantum noise operator can be written as

$$\hat{h}_z = h_g|g\rangle\langle g| + h_e|e\rangle\langle e|,$$

where $h_g = \langle g|\hat{h}_z|g\rangle$ and $h_e = \langle e|\hat{h}_z|e\rangle$. The density matrix $\hat{\varrho}$ of the Mn-electron coupled system obeys the master equation

$$\dot{\varrho} = -i[(\omega_M + \hat{h}_z)\hat{M}_z + \omega_0|e\rangle\langle e|,\hat{\varrho}] + \gamma_g\mathcal{D}[|e\rangle\langle g|]\hat{\varrho} + \gamma_e\mathcal{D}[|g\rangle\langle e|]\hat{\varrho}. \tag{8}$$

Due to the coupling $\hat{M}_z\hat{h}_z$, the total magnetic field on the Mn spin is $\omega_M + h_g$ ($\omega_M + h_e$) if the electronic system is in the ground (excited) state. Due to the random hopping of the electronic system between $|g\rangle$ and $|e\rangle$, the total magnetic field on the Mn spin undergoes random jumps between $\omega_M + h_g$ and $\omega_M + h_e$. This randomly fluctuating magnetic field is responsible for the Mn spin pure dephasing.

In the Born-Markov approximation, we obtain the master equation for the Mn spin density matrix:

$$\dot{\rho}(t) = -i[(\omega_M + h_gP_g + h_eP_e)\hat{M}_z,\hat{\rho}(t)] + \Gamma_z\mathcal{D}[\hat{M}_z]\hat{\rho}, \tag{9}$$

where Γ_z follows from Eq. (5) as

$$\Gamma_z = 2\frac{(h_g-h_e)^2}{(\gamma_g+\gamma_e)^2}\frac{\gamma_g\gamma_e}{\gamma_g+\gamma_e}, \tag{10}$$

where $\gamma_g\gamma_e/(\gamma_g+\gamma_e) \sim \min\{\gamma_g,\gamma_e\}$. Equations (9) and (10) are valid when the Mn spin decoherence is much slower than the slowest fluctuation of the electronic system (i.e., $\Gamma_z \ll \min\{\gamma_g,\gamma_e\}$) or equivalently weak coupling $|h_g - h_e| \ll \gamma_g + \gamma_e$. Otherwise, the Born-Markov approximation and hence Eqs. (9) and (10) are no longer valid.

For either the Markovian or non-Markovian regime, we can always map $\hat{h}_z(t)$ to a classical telegraph noise $\tilde{h}(t)$ that starts from h_g (h_e) with probability P_g (P_e) at $t = 0$ and then undergoes random jumps from h_g to h_e (from h_e to h_g) with a rate γ_g (γ_e). Then we have

$$\frac{\rho_{mm'}(t)}{\rho_{mm'}(0)} = e^{-i(m-m')\omega_M t}\langle e^{-i(m-m')\tilde{\varphi}}\rangle,$$

where $\tilde{\varphi} \equiv \int_0^t \tilde{h}(t')dt'$ and $\langle\cdots\rangle$ denotes the average over the noise. Following the method in Ref. [53], we obtain

$$\langle e^{-i\tilde{\varphi}}\rangle = e^{-i(h_g+h_e)t/2}e^{-(\gamma_g+\gamma_e)t/2}\left(e^{\gamma t/2}\frac{1+p}{2} + e^{-\gamma t/2}\frac{1-p}{2}\right) \tag{11}$$

as the sum of two exponential decays, where

$$\gamma = \sqrt{(\gamma_g+\gamma_e)^2 + 2i(h_g-h_e)(\gamma_g-\gamma_e) - (h_g-h_e)^2},$$

$$p \equiv \frac{(\gamma_g+\gamma_e)^2 + i(h_g-h_e)(\gamma_g-\gamma_e)}{(\gamma_g+\gamma_e)\gamma},$$

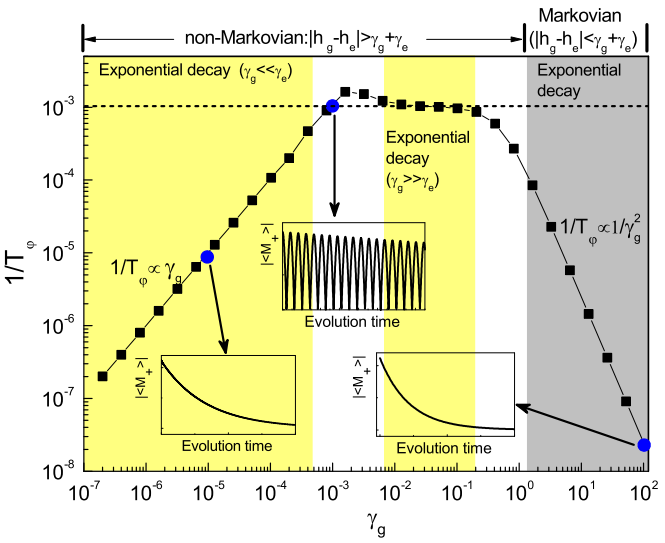

FIG. 1. Mn spin pure dephasing due to the electronic environment, which is modeled as an open two-level system undergoing random hopping between its ground state $|g\rangle$ and excited state $|e\rangle$. The three insets show the real-time evolution of $|\langle\hat{M}_+(t)\rangle|$ at $\gamma_g = 10^{-5}, 10^{-3}$, and 10^2, respectively (as marked by the blue dots), and the dashed line marks $\gamma_e = 10^{-3}$. The unit of energy is $|h_g - h_e|$ and the unit of time is $1/|h_g - h_e|$.

and $\sqrt{z} \equiv \sqrt{|z|}e^{i\,\mathrm{Arg}(z)/2}$ with $\mathrm{Arg}(z) \in (-\pi,\pi]$, while $\langle e^{-i\lambda\tilde{\varphi}}\rangle = \langle e^{-i\tilde{\varphi}}\rangle|_{h_{g,e}\to\lambda h_{g,e}}$. We have verified that the above analytical results agree exactly with the numerical solution to Eq. (8) up to the machine accuracy. This suggests that the mapping from $\hat{h}_z(t)$ to $\tilde{h}(t)$ is exact, consistent with the absence of backaction from the Mn spin onto the electronic environment.

C. Dephasing in Markovian and non-Markovian regimes

Here we discuss two limiting cases:

$$\langle e^{-i\tilde{\varphi}}\rangle \approx \begin{cases} e^{i(h_g P_g + h_e P_e)t} e^{-\Gamma_z t/2} & (|h_g - h_e| \ll \gamma_g + \gamma_e), \\ \sum\limits_{\alpha=g,e} e^{-ih_\alpha t} e^{-\gamma_\alpha t} P_\alpha & (|h_g - h_e| \gg \gamma_g + \gamma_e). \end{cases} \tag{12}$$

The weak-coupling (or equivalently Markovian) regime $|h_g - h_e| \ll \gamma_g + \gamma_e$ recovers Eqs. (9) and (10), where the Mn spin precesses with a single frequency $\omega_M + h_g P_g + h_e P_e$ and its first-order phase coherence decays exponentially with rate $\Gamma_z/2$. In the strong coupling (or equivalently strong non-Markovian) regime $|h_g - h_e| \gg \gamma_g + \gamma_e$, the Mn spin has a probability P_g (P_e) to precess with frequency $\omega_M + h_g$ ($\omega_M + h_e$) and its first-order phase coherence decays exponentially with rate γ_g (γ_e). The interference between $e^{-ih_g t}$ and $e^{-ih_e t}$ gives rise to rapid modulation at frequency $|h_g - h_e|$:

$$|\langle e^{-i\tilde{\varphi}}\rangle| = \sqrt{(e^{-\gamma_g t} P_g + e^{-\gamma_e t} P_e)^2 - 4e^{-\gamma_g t} P_g e^{-\gamma_e t} P_e \sin^2 \frac{(h_g - h_e)t}{2}}.$$

The modulation is pronounced when γ_g and γ_e are comparable; e.g., $\gamma_g = \gamma_e$ gives the maximal modulation $|\langle e^{-i\tilde{\varphi}}\rangle| = e^{-\gamma_g t}|\cos[(h_g - h_e)t/2]|$. In terms of the Fourier transform of $\rho_{m,m+1}(t)$, i.e., the absorption spectrum of the Mn spin, the strong non-Markovian regime corresponds to two absorption lines at $\omega_M + h_g$ (weight P_g and linewidth γ_g) and $\omega_M + h_e$ (weight P_e and linewidth γ_e), with their separation $|h_g - h_e|$ much larger than their total broadening $\gamma_g + \gamma_e$. When we increase γ_g, γ_e so that their total broadening $\gamma_g + \gamma_e$ is much larger than their separation $|h_g - h_e|$, we enter the Markovian regime, where the two absorption lines merge into a single line at $\omega_M + h_g P_g + h_e P_e$ and the linewidth $\Gamma_z/2$ decreases with further increase of γ_g, γ_e. This underlies the so-called "motional narrowing" phenomena in NMR spectroscopy [54].

For simplicity we always fit the decay of the upper envelope of the first-order coherence $|\rho_{m,m+1}(t)|$ by a single exponential e^{-t/T_φ}, which defines the Mn spin pure dephasing time T_φ. Equation (11) shows that in general $|\rho_{m,m+1}(t)|$ and hence $1/T_\varphi$ depend on three parameters: γ_g, γ_e, and $|h_g - h_e|$. Equation (12) shows that in the Markovian regime, $1/T_\varphi = \Gamma_z/2$, while in the strong non-Markovian regime, $1/T_\varphi$ is roughly equal to the decay rate of the dominantly occupied electronic state, i.e., $1/T_\varphi \approx \gamma_g$ when $\gamma_e \gg \gamma_g$ (and hence $P_g \gg P_e$) and $1/T_\varphi \approx \gamma_e$ when $\gamma_g \gg \gamma_e$ (and hence $P_e \gg P_g$).

First we discuss the dependence of $1/T_\varphi$ on $|h_g - h_e|$. Suppose we fix γ_g, γ_e and increase $|h_g - h_e|$ gradually, starting from the Markovian regime $|h_g - h_e| \ll \gamma_g + \gamma_e$. Then the Mn spin undergoes exponential dephasing with a rate that increases rapidly as $1/T_\varphi \propto |h_g - h_e|^2$. When $|h_g - h_e|$ becomes comparable to $\gamma_g + \gamma_e$—the onset of the non-Markovian regime—the pure dephasing rate reaches $1/T_\varphi \sim \min\{\gamma_g, \gamma_e\}$ and pronounced modulation appears in the dephasing profile, which is the sum of two exponential functions [see Eq. (11)]. Upon further increase of $|h_g - h_e|$ such that it becomes much larger than $\gamma_g + \gamma_e$, we enter the strong non-Markovian regime, where the Mn spin pure dephasing rate remains $1/T_\varphi \approx \min\{\gamma_g, \gamma_e\}$. These results are summarized as

$$\frac{1}{T_\varphi} \approx \begin{cases} \frac{(h_g - h_e)^2}{(\gamma_g + \gamma_e)^2} \frac{\gamma_g \gamma_e}{\gamma_g + \gamma_e} & (|h_g - h_e| \ll \gamma_g + \gamma_e), \\ \min\{\gamma_g, \gamma_e\} & (|h_g - h_e| \gg \gamma_g + \gamma_e). \end{cases} \tag{13}$$

An important observation is that the Mn spin pure dephasing rate $1/T_\varphi$ will never exceed the rate of the slowest fluctuation of the electronic environment.

Next we turn to the dependence of $1/T_\varphi$ on γ_g and γ_e. Since γ_g and γ_e are symmetric, we need only consider the dependence on γ_g for fixed γ_e. In Fig. 1, we set $|h_g - h_e| = 1$ (i.e., taking $|h_g - h_e|$ as the unit of energy so that the unit of time is $1/|h_g - h_e|$), fix $\gamma_e = 10^{-3}$, and plot $1/T_\varphi$ as a function of γ_g. When we start from $\gamma_g \gg |h_g - h_e|$ (i.e., the Markovian regime) and gradually decrease γ_g, the Mn spin undergoes exponential dephasing (see the bottom-right inset of Fig. 1) with a rate that increases rapidly as $1/T_\varphi \approx \Gamma_z/2 \propto 1/\gamma_g^2$. When γ_g becomes comparable with $|h_g - h_e|$—the onset of the

non-Markovian regime—pronounced modulations appear in the dephasing profile and the characteristic pure dephasing rate reaches $1/T_\varphi \sim \gamma_e$. Upon further decrease of γ_g well below $|h_g - h_e|$, we enter the strong non-Markovian regime, where the Mn spin pure dephasing rate is roughly equal to the decay rate of the dominantly occupied electronic state; i.e., when $\gamma_g \gg \gamma_e$, the Mn spin undergoes exponential dephasing with a rate $1/T_\varphi \approx \gamma_e$; when γ_g becomes comparable with γ_e, strong modulation appears in the dephasing profile (see the upper inset of Fig. 1); when γ_g drops well below γ_e, the dephasing profile becomes exponential again (see the bottom-left inset of Fig. 1) and the dephasing rate $1/T_\varphi \approx \gamma_g$ decreases linearly with γ_g. These results can be summarized as

$$\frac{1}{T_\varphi} \approx \begin{cases} [(h_g - h_e)^2/\gamma_g^2]\gamma_e & (|h_g - h_e| \ll \gamma_g), \\ \gamma_e & (\gamma_e \ll \gamma_g \ll |h_g - h_e|), \\ \gamma_g & (\gamma_g \ll \gamma_e \ll |h_g - h_e|). \end{cases}$$

The above discussions suggest two methods to suppress the Mn spin pure dephasing: (i) Reducing the amount of jump $|h_g - h_e|$ of the effective magnetic field on the Mn spin when the electronic environment jumps randomly between difference states. This can be achieved by placing the Mn spin at certain high-symmetry "sweet spots" or by properly manipulating the electron wave function. (ii) Increasing the fluctuation rates γ_g, γ_e of the electronic system in the weak-coupling (or equivalently Markovian) regime, or decreasing the fluctuation rate of the electronic system in the strong-coupling (or equivalently strong non-Markovian) regime. In the next section, we demonstrate these ideas by performing numerical simulations for the Mn spin pure dephasing caused by two kinds of fluctuations of the electronic system: (1) thermal excitation of an extra electron in a negatively charged QD; (2) optical pumping of a negatively charged QD.

III. Mn SPIN PURE DEPHASING BY ELECTRONIC ENVIRONMENT

A. An extra electron: Thermal fluctuation

1. Theoretical model

Here the electronic environment is an extra electron in a negatively charged QD under an external magnetic field B. The thermal fluctuation of this electron originates from its coupling to acoustic phonons described by $\hat{H}_p = \sum_{\mathbf{q},\lambda} \omega_{\mathbf{q},\lambda} \hat{a}^\dagger_{\mathbf{q},\lambda} \hat{a}_{\mathbf{q},\lambda}$ through the interaction $\hat{H}_{e-p} = \sum_{\mathbf{q},\lambda} M_{\mathbf{q},\lambda} (\hat{a}_{\mathbf{q},\lambda} + \hat{a}^\dagger_{-\mathbf{q},\lambda}) e^{i\mathbf{q}\cdot\mathbf{r}}$, where $\hat{a}^\dagger_{\mathbf{q},\lambda}$ ($\hat{a}_{\mathbf{q},\lambda}$) is creation (annihilation) operator of the acoustic phonon mode of wave vector $\mathbf{q}$ and branch λ. The most relevant interactions between the electron and acoustic phonons include the deformation potential and piezoelectric interactions. In the literature, there is some inconsistency about their expressions [46,55–58], so we give the derivation of these interactions in Appendix A for completeness. The essentially physical picture for the thermal fluctuation is captured by including the ground electron orbital $|1\rangle$ and the first excited electron orbital $|2\rangle$, whose wave functions and energies are $\psi_1(\mathbf{r})$, $\psi_2(\mathbf{r})$ and E_1, E_2, respectively. The orbital excitation energy is $\omega_0 \equiv E_2 - E_1$ and the electron Hamiltonian is $\hat{H}_e = \omega_0 |2\rangle\langle 2| + \omega_e \hat{S}_{e,z}$, where $\omega_e = g_e \mu_B B$ is the electron Zeeman splitting. This model is justified when the temperature

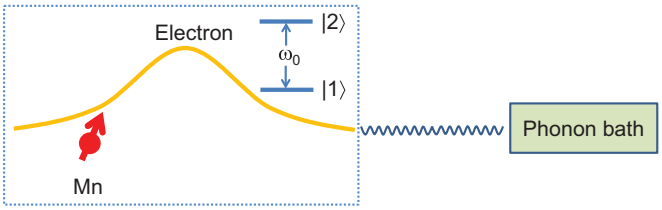

FIG. 2. Sketch of a single Mn spin coupled to an extra electron in the QD through *s-d* exchange interaction. The electron is further coupled to the phonon bath through deformation potential and/or piezoelectric interactions. The effect of the phonon bath is Markovian, so it can be eliminated via the Born-Markov approximation to arrive at a closed, Lindblad master equation for the electron-Mn coupled system.

is small compared with the electron orbital level spacing, so that only the lowest two orbitals have non-negligible thermal occupation.

Now we include the Mn spin and its *s-d* exchange interaction $\hat{\mathbf{M}} \cdot \hat{\mathbf{h}}$ with the electron, where $\hat{\mathbf{h}} = -J_e \hat{\mathbf{S}}_e \delta(\hat{\mathbf{r}}_e - \mathbf{R})$ [see Eq. (1)]. As sketched in Fig. 2, the Mn spin, the electron, and the acoustic phonon bath form a closed quantum system described by the total Hamiltonian $\omega_M \hat{M}_z + \hat{H}_e + \hat{\mathbf{M}} \cdot \hat{\mathbf{h}} + \hat{H}_p + \hat{H}_{e-p}$. As the spectral width of the acoustic phonons is much larger than the phonon-induced electron spin decoherence rate, the phonon bath is Markovian, so we are justified in applying the Born-Markov approximation to eliminate the phonon bath and obtain a closed Lindblad master equation for the electron-Mn coupled system [59,60]. Here we are interested in the Mn spin pure dephasing, so we further neglect the electron-mediated energy exchange between the Mn spin and the phonon bath (which is responsible for the phonon-induced Mn spin relaxation [46]), so that the master equation takes a particularly simple form:

$$\dot{\varrho} = -i[\omega_M \hat{M}_z + \hat{H}_e + \hat{\mathbf{M}} \cdot \hat{\mathbf{h}}, \hat{\varrho}] + (\bar{n} + 1)\gamma \mathcal{D}[|1\rangle\langle 2|]\hat{\varrho} + \bar{n}\gamma \mathcal{D}[|2\rangle\langle 1|]\hat{\varrho}, \quad (14)$$

where the last two terms account for the phonon-induced electron orbital transition from $|2\rangle$ to $|1\rangle$ with rate $(\bar{n}+1)\gamma$ and from $|1\rangle$ to $|2\rangle$ with rate $\bar{n}\gamma$. Here $\bar{n} = 1/(e^{\omega_0/(k_B T)} - 1)$ is the phonon occupation number, T is the temperature of the phonon bath, and $\gamma = 2\pi \sum_{\mathbf{q},\lambda} \delta(\omega_{\mathbf{q},\lambda} - \omega_0) |M_{\mathbf{q},\lambda} \int d\mathbf{r} \psi_2^*(\mathbf{r}) e^{i\mathbf{q}\cdot\mathbf{r}} \psi_1(\mathbf{r})|^2$ is the spontaneous phonon emission rate.

2. Physical picture: Two-level model

Here we present an analytical analysis about the Mn spin pure dephasing by reducing Eq. (14) to the standard two-level model. First, the term $\hat{M}_x \hat{h}_x + \hat{M}_y \hat{h}_y \propto \hat{M}_+ \hat{S}_{e,-} + \text{H.c.}$ (responsible for electron-Mn spin cross relaxation) can be neglected since it involves a large energy mismatch $\omega_e - \omega_M = (g_e - g_{Mn})\mu_B B$. Second, within the subspace spanned by $|1\rangle$ and $|2\rangle$, we have

$$\hat{h}_z = -\hat{S}_{e,z}(J_{11}|1\rangle\langle 1| + J_{22}|2\rangle\langle 2| + J_{12}|1\rangle\langle 2| + J_{12}^*|2\rangle\langle 1|),$$

where $J_{ij}(\mathbf{R}) = J_e \psi_i^*(\mathbf{R}) \psi_j(\mathbf{R})$. The term $J_{12}|1\rangle\langle 2| + J_{12}^*|2\rangle\langle 1|$ involves a large energy mismatch $\pm\omega_0$, so it can also be neglected. In the subsequent numerical simulations,

TABLE I. Parameters used in our numerical calculation, including the effective mass of the electron and the hole (from Ref. [66]), the size of the QD, the g factors of the electron and the Mn spin (from Refs. [7,16]), and the *sp-d* exchange constants (from Ref. [44]). Here m_0 is the mass of a free electron, $\Omega = a^3/4$ is the unit cell volume, and $a = 0.6482$ nm is the lattice constant of CdTe.

m_e^*	m_h^*	L_x	L_y	L_z	g_e	g_M	J_e/Ω	J_h/Ω
$0.1m_0$	$0.493m_0$	24 nm	20 nm	3 nm	-1.67	2.02	0.22 eV	-0.88 eV

we take the initial spin state of the electron to be spin down, so we can further replace the conserved quantity $\hat{S}_{e,z}$ by its initial value $-1/2$. After these approximations, the *s-d* exchange interaction simplifies to

$$\hat{\mathbf{M}}\cdot\hat{\mathbf{h}} \to \hat{M}_z\hat{h}_z \approx \frac{1}{2}\hat{M}_z(J_{11}|1\rangle\langle 1| + J_{22}|2\rangle\langle 2|); \tag{15}$$

thus Eq. (14) reduces to the two-level model [Eq. (8)], with

$$|g\rangle = |1\rangle, \quad |e\rangle = |2\rangle, \tag{16a}$$

$$h_g = \frac{J_{11}}{2}, \quad h_e = \frac{J_{22}}{2}, \tag{16b}$$

$$\gamma_g = \bar{n}\gamma, \quad \gamma_e = (\bar{n}+1)\gamma. \tag{16c}$$

Then all the analytical results and discussions in Sec. II B as well as Fig. 1 are applicable. For example:

(1) Markovian regime $|J_{11} - J_{22}|/2 \ll (2\bar{n}+1)\gamma$. The first-order Mn spin coherence $|\rho_{m,m+1}|$ decays exponentially with a rate

$$\frac{1}{T_\varphi} = \frac{\Gamma_z}{2} = \frac{1}{4}\frac{(J_{11}-J_{22})^2}{\gamma}\frac{\bar{n}(\bar{n}+1)}{(2\bar{n}+1)^3} \tag{17}$$

that is proportional to $\bar{n}$ when $\bar{n} \ll 1$ (i.e., at low temperature) or proportional to $1/\bar{n}$ when $\bar{n} \gg 1$ (i.e., at high temperature). As a function of $\bar{n}$, the maximal pure dephasing rate $\approx (J_{11} - J_{22})^2/(40\gamma)$ occurs at $\bar{n} = (\sqrt{3}-1)/2 \approx 0.37$. Beyond this critical value, further increasing the temperature will suppress the Mn spin pure dephasing, reminiscent of the "motional narrowing" phenomenon in NMR spectroscopy [54].

(2) Strong non-Markovian regime $|J_{11} - J_{22}|/2 \gg (2\bar{n}+1)\gamma$. For $\bar{n} \ll 1$, the Mn spin coherence $|\rho_{m,m+1}|$ decays exponentially with a rate $1/T_\varphi \approx \bar{n}\gamma$. For $\bar{n} \gg 1$, pronounced modulations appear, but the characteristic decay rate is still $1/T_\varphi \sim \bar{n}\gamma$.

In general, the Mn spin pure dephasing is determined by three key parameters: $h_g - h_e = (J_{11} - J_{22})/2$, $\bar{n}$ (or equivalently the temperature $k_B T/\omega_0$), and γ. The first parameter is determined by the size of the QD and the position of the Mn spin in the QD. The second parameter is determined by the size of the QD and the temperature. The third parameter γ, i.e., the spontaneous phonon emission rate, has been studied both theoretically and experimentally in previous works [61–65] and turns out to depend strongly on the semiconductor material and the details of the QD sample, ranging from $\sim$1 ns to $\sim$1 ps [63–65]. Here, in order to focus on the more interesting dependence of the Mn spin dephasing on the Mn spin position and other parameters, we regard γ as a fixed parameter.

3. *Numerical results and discussion*

We consider a flat CdTe QD inside the ZnTe substrate. The valence band offset $\sim$100 meV and the conduction band offset $\sim$800 meV between CdTe and ZnTe are both much larger than the typical confinement energy $\sim$10 meV for the electron and the heavy hole; thus the electron and hole states can be described by a "box" model [44], with the height L_z, length L_x, and width L_y. The electron or heavy-hole ground orbital $\psi_1(\mathbf{r}) = \varphi_1(x)\varphi_1(y)\varphi_1(z)$ and the first excited orbital $\psi_2(\mathbf{r}) = \varphi_2(x)\varphi_1(y)\varphi_1(z)$, where

$$\varphi_n(x) = \sqrt{\frac{2}{L_x}}\sin\frac{n\pi x}{L_x}\ (n = 1,2),$$

$$\varphi_1(y) = \sqrt{\frac{2}{L_y}}\sin\frac{\pi y}{L_y},$$

$$\varphi_1(z) \equiv \sqrt{\frac{2}{L_z}}\sin\frac{\pi z}{L_z}.$$

The parameters used in our numerical calculation are listed in Table I, from which we obtain the *s-d* exchange coefficient $J_e \approx 15$ meV nm^3, the *p-d* exchange coefficient $J_h \approx -60$ meV nm^3, and the electron orbital excitation energy $\omega_0 = 3\pi^2/(2m_e^* L_x^2) \approx 19.6$ meV ≈ 30 ps^{-1}, corresponding to a temperature $\sim$220 K.

Our numerical results are obtained by solving numerically the master equation [Eq. (14)] for the Mn-electron coupled system (see Appendix B for the details). Once the density matrix $\hat{\varrho}(t)$ of the electron-Mn coupled system and hence the Mn spin density matrix $\hat{\rho}(t) = \mathrm{Tr}_e\,\hat{\varrho}(t)$ have been obtained, the Mn spin pure dephasing time T_φ can be obtained by fitting the decay of the real-time evolution of the Mn spin coherence $|\langle\hat{M}_+(t)\rangle|$ by a single exponential e^{-t/T_φ}, where $\hat{M}_+ \equiv \hat{M}_x + i\hat{M}_y$. In the numerical simulations, we start from a coherent superposition $(|-5/2\rangle + |-3/2\rangle)/\sqrt{2}$ of the Mn spin Zeeman eigenstates $\{|m\rangle\}$ ($m = \pm 1/2, \pm 3/2, \pm 5/2$) and spin-down state of the electron (with thermal populations on the ground and first excited orbitals); thus $|\langle M_+(t)\rangle| = \sqrt{5}|\rho_{-5/2,-3/2}(t)|$ and $|\langle M_+(0)\rangle| = \sqrt{5}/2$.

First, our numerical simulations show that the Mn spin T_φ is almost independent of the external magnetic field; e.g., at $T = 50$ K, we always have $T_\varphi \approx 0.07$ μs over the entire range of magnetic field up to $B = 10$ T. This behavior is consistent with the two-level model analysis in Sec. III A 2, but is in sharp contrast to the dramatic reduction of T_1 of the Mn spin upon increasing the magnetic field [46]. Physically, this qualitative difference originates from the different energy mismatches involved in the Mn spin relaxation and Mn spin pure dephasing processes: the former is caused by the electron-Mn spin flip-flop and involves a Zeeman energy mismatch $\omega_e - \omega_M$, which must be dissipated by the phonon modes at the frequency $\omega_e - \omega_M$. Therefore, the significant increase of the phonon density of states with increasing frequency speeds up the

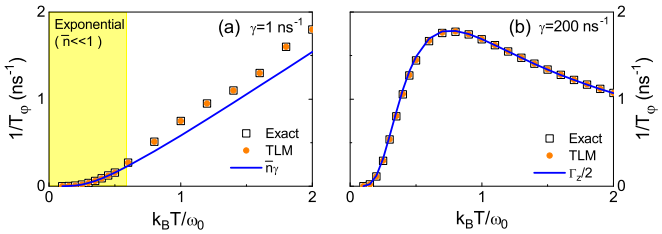

FIG. 3. Pure dephasing rate $1/T_\varphi$ of the Mn spin as a function of temperature under an external magnetic field $B = 1.5$ T and different spontaneous phonon emission rates: (a) $\gamma = 1$ ns^{-1}, (b) $\gamma = 200$ ns^{-1}. The Mn spin locates at $(X,Y,Z) = (11.5,10.5,1.6)$ nm (i.e., near the center of the QD), corresponding to $J_{11} \approx 124$ ns^{-1}, $J_{12} = J_{21} \approx 16$ ns^{-1}, and $J_{22} \approx 2$ ns^{-1}. The coupled master equation [Eq. (14)] is solved exactly (empty squares) or under the approximation Eq. (15) (filled circles). The solid lines in (a) and (b) denote, respectively, the analytical expression for $1/T_\varphi$ in the strong non-Markovian regime and Markovian regime.

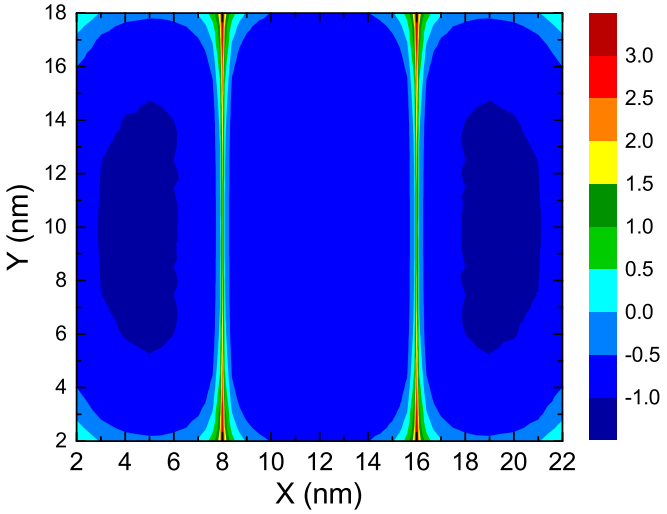

FIG. 4. $\log_{10} T_\varphi$ (T_φ in units of μs) as a function of the lateral position (X,Y) of the Mn ion. The magnetic field $B = 1.5$ T and temperature $T = 50$ K.

electron-Mn spin flip-flop with increasing magnetic field. By contrast, the pure dephasing involves no energy mismatch, so it is insensitive to the magnetic field.

Second, we show the dependence of the Mn spin pure dephasing rate $1/T_\varphi$ on the temperature in Fig. 3, where $1/T_\varphi$ is fitted numerically by solving the master equation [Eq. (14)] for the Mn-electron coupled exactly (empty squares) or under the approximation in Eq. (15) (filled circles). The quantitative agreement between these two results suggest that Eq. (15) serves as an excellent approximation. In Fig. 3(a), we have $|h_g - h_e| = |J_{11} - J_{22}|/2 \approx 61$ ns^{-1} and $\gamma_g + \gamma_e = (2\bar{n}+1)$ns^{-1}; thus the crossover between the Markovian and non-Markovian regimes occurs at $\bar{n} \approx k_B T/\omega_0 \approx 30$. Therefore, the electron environment is non-Markovian over the entire range of temperatures shown in Fig. 3(a). As discussed in Sec. III A 2, the Mn spin coherence $|\langle \hat{M}_+(t)\rangle|$ exhibits exponential decay with a rate $\bar{n}\gamma$ when $\bar{n} \ll 1$ (shaded region). When the temperature increases to $\bar{n} \gg 1$, pronounced modulations appear in the dephasing profile, and the characteristic pure dephasing rate increases linearly with temperature: $1/T_\varphi \sim \bar{n}\gamma \approx \gamma k_B T/\omega_0$. In Fig. 3(b), the electron total dissipation rate $\gamma_g + \gamma_e = 200(2\bar{n}+1)$ ns^{-1} is always much larger than $|h_g - h_e| \approx 61$ ns^{-1}; thus the electron environment is Markovian and the Mn spin coherence $|\langle M_+(t)\rangle|$ undergoes exponential decay at a rate well described by the analytical expression [Eq. (17)] in the Markovian regime. As discussed in Sec. III A 2, at high temperatures ($\bar{n} \gg 1$), the dephasing rate begins to decrease with increasing temperature, reminiscent of the "motional narrowing" phenomenon in NMR spectroscopy.

Third, we consider a most interesting point, i.e., the dependence of the Mn spin T_φ on the position $\mathbf{R} \equiv (X,Y,Z)$ of the Mn spin, which determines

$$|h_g - h_e| = \frac{|J_{11} - J_{22}|}{2} = J_e[\varphi_1^2(X) - \varphi_2^2(X)]\varphi_1^2(Y)\varphi_1^2(Z).$$

When $X = L_x/3$ or $2L_x/3$, we have $|\varphi_1(X)| = |\varphi_2(X)|$ and hence $|h_g - h_e| = 0$. At these two "sweet spots", the phonon-induced random jump of the electron between the ground orbital and the first excited orbital does not change the effective magnetic field on the Mn spin, so the Mn spin dephasing time should be strongly enhanced, as confirmed by our numerical simulations in Fig. 4, where T_φ of the Mn spin is prolonged dramatically near the two sweet spots: $X = 8$ nm and $X = 16$ nm. In addition, the Mn spin T_φ is also enhanced when the Mn spin locates at the edges of the QD, which trivially follows from the vanishing electron density (and hence vanishing J_{11} and J_{22}) at the edges of the QD.

4. *Electrical control of Mn spin dephasing*

The key ingredient of the sweet spot mechanism is the overlap of the electron orbital wave function with the localized Mn spin. In practice, it is hard to move the Mn atom in the QD. Instead, a feasible method is to manipulate the electron wave function, e.g., by applying an external, in-plane electric field F. We assume that the electric field is applied along the x axis. For the electron inside a hard-wall "box" (L_x,L_y,L_z), the electric-field-induced electron orbital displacement can only be obtained numerically. To give an analytical analysis, we replace the hard-wall confinement along the x axis with a harmonic oscillator potential $(1/2)m_e^*\omega_x^2 x^2$, where ω_x is determined by $L_x/2 \equiv 1/\sqrt{m_e^*\omega_x}$. Applying an electric field F shifts the equilibrium position of the electron to

$$x_0 \equiv \frac{eF}{m_e^*\omega_x^2} = F\frac{em_e^*L_x^4}{16} \approx 2.7 \text{ nm} \times \frac{F}{\text{kV/cm}}; \qquad (18)$$

i.e., increasing the electric field by every 1 kV/cm shifts the equilibrium position of the electron by 2.7 nm. Using

$$\frac{J_{22}}{J_{11}} = \left(\frac{\varphi_2(X)}{\varphi_1(X)}\right)^2 = \frac{8(X-x_0)^2}{L_x^2},$$

the sweet spot condition $J_{22} = J_{11}$ is achieved when the electric field is chosen such that $x_0 = X \pm L_x/(2\sqrt{2})$. For example, for the Mn spin located at $X = 0$, the sweet spot condition is satisfied by applying an electric field $F \approx 3$ kV/cm. In Fig. 5, we plot the pure dephasing rate $1/T_\varphi$ of the Mn spin located at the center of the QD as a function of the applied

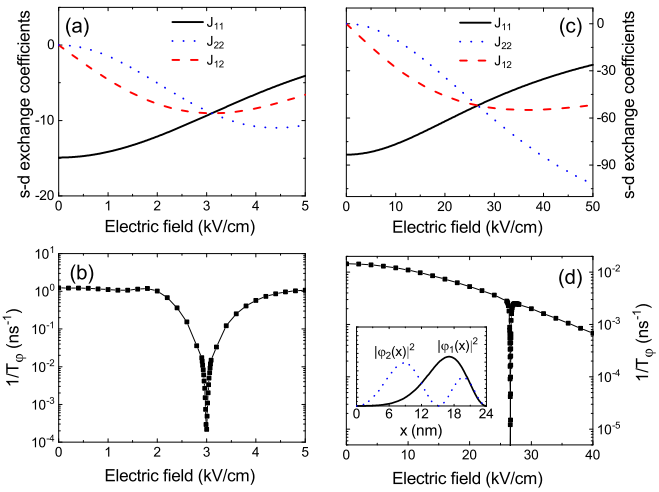

FIG. 5. Electron-Mn *s-d* exchange coefficients and Mn spin pure dephasing rate $1/T_\varphi$ as functions of the applied electric field under a magnetic field $B = 1.5$ T and temperature $T = 50$ K. (a) and (b): The electron is confined in a 3D harmonic oscillator potential $(1/2)m_e^*(\omega_x^2x^2 + \omega_y^2y^2 + \omega_z^2z^2)$ with ω_α determined by $L_\alpha/2 = 1/\sqrt{m_e^*\omega_\alpha}$. (c) and (d): The electron is confined in a 3D hard-wall potential. The inset of (d) shows the electron density distribution at $F \approx 27$ kV/cm for the ground orbital and the first excited orbital. Other parameters are listed in Table I.

electric field along the x axis. When the electron is confined in a harmonic oscillator potential [Figs. 5(a) and 5(b)], the "sweet spot" condition is indeed met at $F \approx 3$ kV/cm. Correspondingly, $1/T_\varphi$ shows a sharp dip at $F \approx 3$ kV/cm, corresponding to $T_\varphi > 1$ μs near the dip. When the electron is confined in a hard-wall "box" [Figs. 5(c) and 5(d)], applying an electric field $F \approx 27$ kV/cm shifts the electron ground orbital and first excited orbital to the sweet spot condition $|\varphi_1(X)| = |\varphi_2(X)|$, so that $J_{11} = J_{22}$ and hence the Mn spin T_φ is significantly prolonged. Here the critical electric field for the "box" model is much larger than that for the harmonic potential, because the hard-wall "box" potential makes it more difficult to shift the electron orbitals. In realistic experiments, the sweet spot condition depends on the specific size and shape of the dot. The results from the harmonic oscillator model and the "box" model can be taken as the lower bound and upper bound of the required electric field.

B. Negatively charged QD under optical pumping

1. Theoretical model

Experimentally, optical pumping is commonly used to initialize, manipulate, and/or readout the Mn spin state [22,27,28,30–38]; thus the Mn spin dephasing due to the fluctuation of the electronic environment during optical pumping is relevant to many experiments. For a negatively charged QD, optical pumping excites the single-electron ground orbital $|1\rangle$ to the exciton orbital $|2\rangle$, which consists of two electrons in the spin singlet state and an extra heavy hole. The extra electron in the ground orbital is coupled to the Mn spin through the isotropic *s-d* exchange interaction $-J_e|\psi_1(\mathbf{R})|^2\hat{\mathbf{M}}\cdot\hat{\mathbf{S}}_e$ [cf. Eq. (1)], where $\hat{\mathbf{S}}_e$ is the electron spin and $\psi_1(\mathbf{r})$ is the wave function of $|1\rangle$. The extra heavy hole in the exciton is coupled to the Mn spin through the Ising-like *p-d* exchange interaction $-(J_h/3)|\psi_2(\mathbf{R})|^2\hat{M}_z\hat{S}_{h,z}$ [cf. Eq. (2)], where $\hat{\mathbf{S}}_h$ is the spin of the heavy hole ($\hat{S}_{h,z} = \pm 3/2$) and $\psi_2(\mathbf{R})$ is the wave function of the heavy hole in the exciton. The total interaction between the Mn spin and the electronic environment can be written as $\hat{\mathbf{M}}\cdot\hat{\mathbf{h}}$, where $\hat{\mathbf{h}} = -J_e|\psi_1(\mathbf{R})|^2\hat{\mathbf{S}}_e|1\rangle\langle 1| - (J_h/3)|\psi_2(\mathbf{R})|^2\hat{S}_{h,z}\mathbf{e}_z|2\rangle\langle 2|$. Under optical pumping, the electronic system jumps randomly between the ground orbital and the exciton orbital, leading to random fluctuation of the effective magnetic field $\hat{\mathbf{h}}$ on the Mn spin. The fluctuation of $\hat{h}_x, \hat{h}_y$ leads to Mn spin relaxation, while the fluctuation of $\hat{h}_z$ leads to Mn spin pure dephasing. The former have been studied by a series of works [29,30,44,67,68], while the latter has not been discussed so far. Thus we focus on the Mn spin pure dephasing and drop h_x and h_y; then the electron spin $\hat{S}_{e,z}$, the heavy-hole spin $\hat{S}_{h,z}$, and the Mn spin $\hat{M}_z$ are all conserved. We assume the electronic environment is initially in the spin-down ground state $|g\rangle \equiv |1,\downarrow\rangle$ with $\hat{S}_{e,z} = -1/2$; then optical pumping creates the spin-down exciton state $|e\rangle \equiv |2,\downarrow\uparrow\Downarrow\rangle$ with $\hat{S}_{h,z} = -3/2$, where $|\uparrow\rangle, |\downarrow\rangle$ are the electron spin-up and spin-down states and $|\Downarrow\rangle$ is the spin-down state of the heavy hole. Therefore, the *sp-d* exchange interaction between the electronic environment and the Mn spin simplifies to

$$\hat{\mathbf{M}}\cdot\hat{\mathbf{h}} \to \hat{M}_z\hat{h}_z \approx \hat{M}_z(J_{11}|g\rangle\langle g| + J_{22}|e\rangle\langle e|),$$

where $J_{11} \equiv (1/2)J_e|\psi_1(\mathbf{R})|^2$ and $J_{22} = (1/2)J_h|\psi_2(\mathbf{R})|^2$.

Under continuous optical pumping, the Hamiltonian of the electronic environment is $\hat{H}_e(t) = \omega_0|e\rangle\langle e| + (\Omega_R/2)(e^{-i\omega t}|e\rangle\langle g| + e^{i\omega t}|g\rangle\langle e|)$, where ω_0 is the exciton excitation energy, Ω_R is the Rabi frequency, and ω is the optical pumping frequency. In the rotating frame, the electronic Hamiltonian becomes

$$\hat{H}_e = \Delta|e\rangle\langle e| + \frac{\Omega_R}{2}(|e\rangle\langle g| + |g\rangle\langle e|),$$

where $\Delta \equiv \omega_0 - \omega$ is the detuning of the optical pumping. The density matrix $\hat{\varrho}(t)$ of the Mn spin and the electronic environment obeys the Lindblad master equation

$$\dot{\varrho} = -i[\omega_M\hat{M}_z + \hat{H}_e + \hat{M}_z\hat{h}_z, \hat{\varrho}] + \gamma_1\mathcal{D}[|g\rangle\langle e|]\hat{\varrho} + \gamma_\phi\mathcal{D}[|e\rangle\langle e|]\hat{\varrho}, \quad (19)$$

where γ_1 (γ_ϕ) is the spontaneous emission (pure dephasing) rate of the exciton. By solving this equation numerically, we can find $\hat{\varrho}(t)$ and hence the Mn spin coherence $|\langle\hat{M}_+(t)\rangle| = |\mathrm{Tr}\,\hat{\varrho}(t)\hat{M}_+|$. We always fit the decay envelope of $|\langle\hat{M}_+(t)\rangle|$ by a single exponential e^{-t/T_φ}, which defines the Mn spin dephasing time T_φ. In the numerical simulations, we start from a coherent superposition $(|-5/2\rangle + |-3/2\rangle)/\sqrt{2}$ of the Mn spin Zeeman eigenstates and the single-electron spin-up ground state $|g\rangle$; thus $|\langle\hat{M}_+(t)\rangle| = \sqrt{5}|\rho_{-5/2,-3/2}(t)|$ and $|\langle\hat{M}_+(0)\rangle| = \sqrt{5}/2$.

2. Physical picture: Two-level model

Before going to numerical simulations, we present an analytical study of the Mn spin pure dephasing by reducing Eq. (19) to the standard two-level model. This is possible when $\gamma_\phi \gg \gamma_1$. In this case the off-diagonal elements of $\hat{\varrho}(t)$ decay much faster than the evolution of the diagonal elements of $\hat{\varrho}(t)$. Thus the diagonal elements obey a closed set of

rate equations, as characterized by the optical pumping rate $R \equiv 2\pi(\Omega_R/2)^2\delta^{[(\gamma_1+\gamma_\phi)/2]}(\Delta)$. Thus we recover the standard two-level model, with

$$h_g = J_{11}, \quad h_e = J_{22}, \tag{20a}$$

$$\gamma_g = R, \quad \gamma_e = R + \gamma_1. \tag{20b}$$

Then all the analytical results and discussions in Sec. II B and Sec. III A 2 as well as Fig. 1 are applicable. Moreover, by comparing Eq. (20) to Eq. (16), we see that optical pumping corresponds to thermal excitation of an extra electron with $\gamma \to \gamma_1$ and $\bar{n} \to R/\gamma_1$. Tuning the optical pumping strength can induce the crossover between the Markovian and non-Markovian regimes:

(1) Markovian regime $|J_{11} - J_{22}| \ll 2R + \gamma_1$. The Mn spin coherence $|\langle \hat{M}_+(t)\rangle|$ decays exponentially with a rate

$$\frac{1}{T_\varphi} = \frac{\Gamma_z}{2} = (J_{11} - J_{22})^2 \frac{R(R+\gamma_1)}{(2R+\gamma_1)^3}, \tag{21}$$

consistent with our previous work [69], where we applied the Born-Markov approximation to derive an explicit analytical expression for the optical-pumping-induced pure dephasing of the electron spin in the nitrogen-vacancy center. Equation (21) shows $1/T_\varphi$ is proportional to R when $R \ll \gamma_1$ or proportional to $1/R$ when $R \gg \gamma_1$. As a function of R, the maximal dephasing rate $\approx (J_{11} - J_{22})^2/(10\gamma)$ occurs at $R = (\sqrt{3} - 1)\gamma_1/2 \approx 0.37\gamma_1$. Beyond this critical value, further increase of R can suppress the Mn spin pure dephasing, reminiscent of the "motional narrowing" phenomenon [54].

(2) Strong non-Markovian regime $|J_{11} - J_{22}| \gg 2R + \gamma_1$. For $R \ll \gamma_1$, the Mn spin coherence $|\langle \hat{M}_+(t)\rangle|$ decays exponentially with a rate $1/T_\varphi \approx R$. For $R \gg \gamma_1$, pronounced modulations appear, but the characteristic decay rate is still $1/T_\varphi \sim R$.

3. Numerical results and discussion

For the numerical simulation, we consider 3D harmonic oscillator potential $(1/2)m^*(\omega_x^2 x^2 + \omega_y^2 y^2 + \omega_z^2 z^2)$ for the electron and the heavy hole, where ω_α is determined by the effective QD size $L_z = 4$ nm, $L_x = 24$ nm, $L_y = 20$ nm through $L_\alpha/2 = 1/\sqrt{m^*\omega_\alpha}$, $m^* = m_e^*$ (for the electron) or m_h^* (for the heavy hole), and other parameters are listed in Table I. Here, following Refs. [70,71], we have assumed that the typically weaker confinement potential $\{\omega_\alpha\}$ of the heavy hole compared with the electron (due to the typically smaller valence band offset compared with the conduction band offset [72]) is compensated by its heavy mass, so that the electron and hole have the same effective QD size. We take the detuning $\Delta = 1$ meV and the Mn spin to locate at the center of the QD, i.e., the minimum of the 3D harmonic potential, thus $\psi_1(\mathbf{R}) = \psi_2(\mathbf{R}) = \sqrt{8/(L_x L_y L_z)}/\pi^{3/4}$. Other parameters are listed in Table I, from which we obtain $J_{11} \approx 8.5$ ns^{-1} and $J_{22} \approx -34$ ns^{-1}.

In Fig. 6, we show the Mn spin pure dephasing rate $1/T_\varphi$ as a function of the optical pumping rate R with $\gamma_1 = \gamma_\phi = 1$ns^{-1}. The behavior of $1/T_\varphi$ is determined by three key parameters: $|J_{11} - J_{22}| \approx 42$ ns^{-1}, the spontaneous emission rate $\gamma_1 = 1$ ns^{-1}, and R. The crossover between the Markovian and non-Markovian regimes occurs at $|J_{11} - J_{22}| \approx 2R + \gamma_1$, corresponding to a critical pumping rate $R_c \approx 21$ ns^{-1}, as marked by the dashed line in Fig. 6. Suppose we start from the strong non-Markovian regime $R \ll \gamma_1$ ($\ll |J_{11} - J_{22}|$) and gradually increase R; the Mn spin undergoes exponential decay (see the inset of Fig. 6) with a rate that increases linearly: $1/T_\varphi \sim R$ (see the blue solid line). When R becomes comparable with γ_1, pronounced modulations appear (see the inset of Fig. 6) and the Mn spin dephasing rate remains $1/T_\varphi \sim \gamma_1$ upon further increase of R. When $R \gg R_c$, we enter the Markovian regime and the Mn spin dephasing becomes exponential again (see the inset of Fig. 6) and the decay rate $1/T_\varphi \propto 1/R$ decreases with further increase of R (see the blue solid line in Fig. 6).

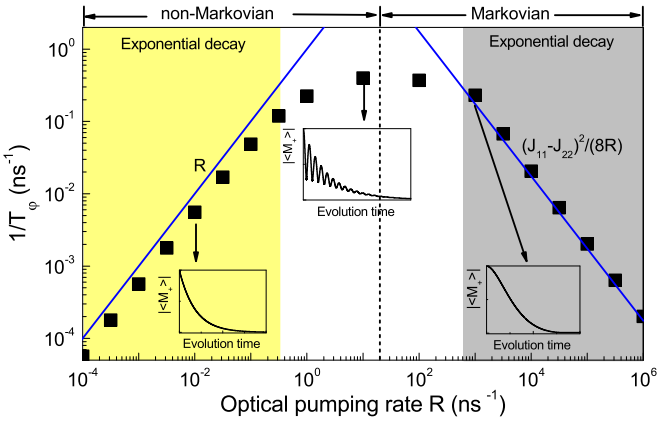

FIG. 6. Mn spin pure dephasing rate $1/T_\varphi$ obtained by numerically solving Eq. (19) as a function of optical pumping rate R, with $\gamma_1 = \gamma_\phi = 1$ ns^{-1}. The solid lines shows non-Markovian limit $1/T_\varphi = R$ and the Markovian approximation $1/T_\varphi = (J_{11} - J_{22})^2/(8R)$. The vertical dashed line marks the crossover point between the Markovian and non-Markovian regimes.

Similar to the case of thermal fluctuation (see Sec. III A 4), the Mn spin dephasing due to optical pumping can also be controlled by applying an external electric field, which shifts the electron and hole envelope functions $\psi_1(\mathbf{r})$ and $\psi_2(\mathbf{r})$ away from the center of the QD (where the Mn spin locates). Consequently, the *sp-d* exchange coefficients J_{11} and J_{22} decrease continuously with increasing electric field, as shown in Fig. 7(a). This in turn could significantly suppress the Mn spin dephasing, as shown in Fig. 7(b). Under strong optical pumping $R = 10^3$ ns^{-1} [black squares and lines in Fig. 7(b)], the electronic environment is Markovian, so the Mn spin pure dephasing rate $1/T_\varphi \propto (J_{11} - J_{22})^2$ decreases continuously with increasing electric field. Under weak optical pumping $R = 10^{-3}$ ns^{-1} [orange squares in Fig. 7(b)], the electronic environment is strongly non-Markovian in zero electric field, so the Mn spin pure dephasing rate remains $1/T_\varphi \approx R$ with increasing electric field, until $|J_{11} - J_{22}|$ becomes comparable with $2R + \gamma_1 \approx \gamma_1$—the crossover from the non-Markovian regime into the Markovian regime [as marked by the arrow in Fig. 7(b)]. Afterwards, further increasing the electric field leads to significant suppression of the Mn spin dephasing according to $1/T_\varphi \propto (J_{11} - J_{22})^2$.

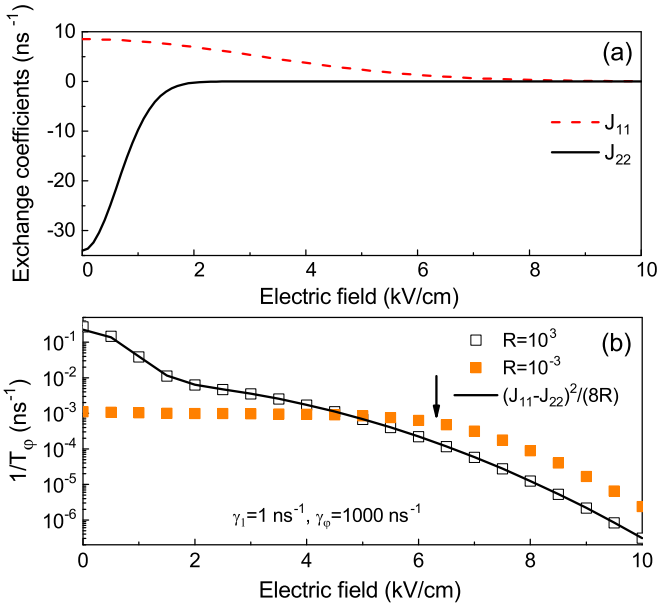

FIG. 7. Electric field control of the *sp-d* exchange coefficients (a) and hence the Mn spin pure dephasing rate (b) under different optical pumping strengths: $R = 10^3$ ns^{-1} (empty squares) and $R = 10^{-3}$ ns^{-1} (filled squares). The black solid lines denotes the analytical approximation Eq. (21) in the Markovian regime for the case $R = 10^3$ ns^{-1}. We take $\gamma_1 = 1$ ns^{-1} and $\gamma_\phi = 1000$ ns^{-1}.

C. Other fluctuations of the electronic environment

In addition to the thermal excitation of the electron and optical pumping of negatively charged excitons, other commonly encountered sources of fluctuation include the thermal excitation of the hole, optical pumping of neutral and positively charged excitons, tunneling between the QD and an electron/hole reservoir nearby, and random flip of the electron/hole spin. Here we briefly discuss the Mn spin pure dephasing caused by these mechanisms based on the two-level model in Sec. II B, which has three key parameters: γ_g, γ_e, and $|h_g - h_e|$. According to the discussions in Sec. II C, the Mn spin pure dephasing rate $1/T_\varphi$ in the Markovian and non-Markovian regimes are summarized in Eq. (13). For specificity we consider the Mn spin located at the center of a CdTe QD described by the "box" model. For the QD size as listed in Table I, the ground orbital and first excited orbital of the hole are the same as those of the electron, but the hole-Mn *p-d* exchange constant $J_h \approx -60$ meV nm^3 is four times that of the electron-Mn *s-d* exchange constant $J_e \approx 15$ meV nm^3; thus $J_{11} \approx 124$ ns^{-1} ($J_{22} \approx 2$ ns^{-1}) for an electron in the ground (first excited) orbital, and $J_{11} \approx 496$ ns^{-1} ($J_{22} \approx 8$ ns^{-1}) for a heavy hole in the ground (first excited) orbital. Since the heavy-hole effective mass m_h^* is about five times that of the electron effective mass m_e^* (see Table I), the orbital excitation energy of the heavy hole is about 4 meV (corresponding to a temperature ~50 K), i.e., 20% that of the electron.

The thermal excitation of the heavy hole corresponds to $|h_g - h_e| = |J_{11} - J_{22}|/2 \approx 244$ ns^{-1}, which is four times that of the electron. For the spontaneous phonon emission rate $\gamma \ll 244$ ns^{-1}, we are always in the non-Markovian regime up to $T = 50$ K, so Eq. (13) gives $1/T_\varphi \approx \gamma$. For $\gamma \gg 244$ns^{-1}, we are always in the Markovian regime; thus $1/T_\varphi$ decreases with increasing γ, e.g., $1/T_\varphi \sim 5$ ns^{-1} at $\gamma = 1$ ps^{-1} and $T = 50$ K.

For the electron or hole tunneling between the QD and an electron/hole reservoir nearby, $|g\rangle$ corresponds to zero electron/hole in the QD, $|e\rangle$ corresponds to one electron/hole in the ground orbital, $\gamma_g = \gamma_e = \Gamma_t$ corresponds to the tunneling rate, and $|h_g - h_e| = |J_{11}|/2$ is 62 ns^{-1} for electron tunneling and 248 ns^{-1} for hole tunneling. For typical tunneling rates $\Gamma_t \sim$ a few kHz (Refs. [39,73]), we are always in the non-Markovian regime; thus $1/T_\varphi \approx \Gamma_t$.

For the electron or hole spin relaxation, $|g\rangle$ and $|e\rangle$ correspond to the spin-down and spin-up states, respectively, $\gamma_g \approx \gamma_e = \gamma_{sf}$ corresponds to the spin-relaxation rate, and $|h_g - h_e| = |J_{11}|$ is 124 ns^{-1} for the electron and 496 ns^{-1} for the heavy hole. Previous experiments at low temperatures have reported an electron spin relaxation rate ranging from ~10 Hz to ~10 kHz (Ref. [39]) and a hole spin relaxation rate ranging from ~100 kHz (Refs. [74,75]) to ~10 MHz (Refs. [76,77]), so we are always in the non-Markovian regime, i.e., $1/T_\varphi \approx \gamma_{sf}$.

Finally, applying an in-plane electron field of a few (or a few tens) of kV/cm can significantly reduce the electron-Mn and hole-Mn coupling coefficients (see Figs. 5 and 7) and hence $|h_g - h_e|$. So we expect the electrical control of the Mn spin pure dephasing due to all the mechanism mentioned above to remain effective.

IV. Mn SPIN DEPHASING BY NUCLEAR SPIN ENVIRONMENT

At low temperature, the thermal fluctuation of the electronic environment and hence the resulting Mn spin dephasing are suppressed. For example, in Fig. 3(a), the Mn spin pure dephasing rate $1/T_\varphi \approx \bar{n}\gamma \approx e^{-\omega_0/(k_B T)}$ ns^{-1} is suppressed exponentially when $k_B T \ll \omega_0$; e.g., $T_\varphi \approx 0.2$ ms for $T \approx 22$ K and $T_\varphi \approx 0.4$ s for $T \approx 11$ K. Even for a much larger spontaneous phonon emission rate $\gamma = 200$ ns^{-1} (Refs. [64,65]), the Mn spin pure dephasing rate [see Fig. 3(b)] $1/T_\varphi \approx (J_{11} - J_{22})^2 e^{-\omega_0/(k_B T)}/(4\gamma)$ at low temperature still becomes very small, e.g., $T_\varphi \approx 26$ ms at $T \approx 11$ K. Therefore, at low temperature, the thermal fluctuation mechanism is not relevant to Mn spin dephasing.

In many quantum information systems (such as semiconductor QDs, phosphorus and bismuth donors in silicon, and nitrogen-vacancy centers in diamond), the nuclear spin environment dominates the dephasing of the central electron spin qubits at low temperature and sets the ultimate limitation to their applications. This motivates us to investigates the Mn spin dephasing caused by the nuclear spin environment.

We consider a single substitutional Mn atom on the Cd site of the CdTe lattice. Only four stable isotopes of Te and Cd have nonzero nuclear spins ($I = 1/2$): ^{111}Cd, ^{113}Cd, ^{123}Te, and ^{125}Te. Their gyromagnetic ratio [in units of 10^6 rad/(T s)] and natural abundance are 56.9 (12.8%), 59.6 (12.2%), 70 (7.1%), and 85.1 (0.9%), respectively. Due to the highly localized nature of the Mn $3d^5$ electrons, these nuclear spins are coupled to the Mn electron spin primarily through the dipolar hyperfine interaction $\hat{\mathbf{M}} \cdot \hat{\mathbf{h}}$, where $\hat{\mathbf{h}}$ is given by Eq. (3). As discussed previously, the fluctuation of $\hat{h}_x, \hat{h}_y$ leads to Mn spin relaxation, while the fluctuation of $\hat{h}_z$ leads to Mn spin pure dephasing.

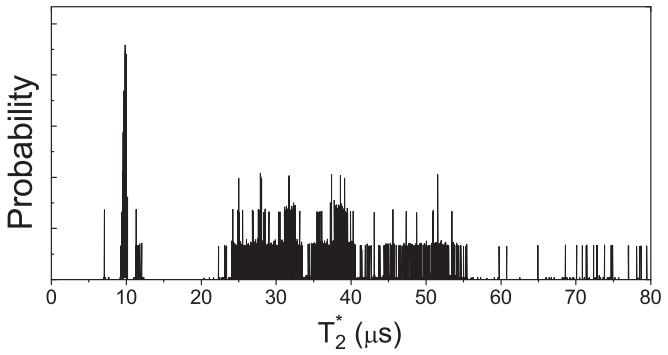

FIG. 8. Distribution of nuclear environment induced T_2^* of the Mn spin, obtained from the statistics of 100 000 repeated simulations for a $9 \times 6 \times 5$ lattice of the CdTe crystal.

Under a moderate magnetic field, the large Zeeman energy mismatch between the Mn spin and the nuclear spin suppresses the Mn-nuclear spin flip-flop and hence the Mn spin relaxation, similar to the suppression of electron spin relaxation induced by nuclear spins in QDs. Then $\hat{\mathbf{M}} \cdot \hat{\mathbf{h}}$ can be replaced by $\hat{M}_z \hat{h}_z$, where $\hat{h}_z = \sum_n \mathbf{a}_n \cdot \hat{\mathbf{I}}_n$ is the nuclear Overhauser field, and

$$\mathbf{a}_n = \sum_n \frac{\mu_0}{4\pi\rho_n^5}\gamma_e\gamma_n\left(-3\rho_{n,x}\rho_{n,z}, -3\rho_{n,y}\rho_{n,z}, \rho_n^2 - 3\rho_{n,z}^2\right).$$

Due to the extremely small magnetic momentum of the nuclear spins, we have $k_B T \gg$ nuclear spin Zeeman splitting even under a strong magnetic field (e.g., a few teslas) and low temperature (e.g., a few kelvins), so the nuclear spins are in the completely random state. Therefore, $\hat{h}_z$ is a random variable with vanishing mean $\langle \hat{h}_z \rangle = 0$ but strong static, thermal fluctuation:

$$\langle \hat{h}_z^2 \rangle = \sum_n \frac{I(I+1)}{3}|\mathbf{a}_n|^2.$$

The resulting Mn spin pure dephasing is referred to as inhomogeneous dephasing and the characteristic time scale can be estimated as $T_2^* \approx 1/\langle \hat{h}_z^2 \rangle^{1/2}$.

Since $|\mathbf{a}_n|^2 \propto 1/\rho_n^6$ decays rapidly with the distance ρ_n, the dominant contribution to $\langle \hat{h}_z^2 \rangle$ comes from those nuclei on the nearest-neighbor Te sites. In our numerical calculation, we find it sufficient to consider a $9 \times 6 \times 5$ CdTe crystal and replace the center Cd atom by the Mn atom. In the worst case, i.e., when the four nearest-neighbor Te sites are all occupied by ^{125}Te, we may neglect the effect of other nuclear spins and obtain $T_2^* \approx 5$ μs. This serves as the lower bound of T_2^* caused by the nuclear spins and agrees qualitatively with the Rabi oscillation decay time ~ 0.5 μs of diluted Mn spins in the MgO crystal [48]. In practice, we obtain different T_2^* for different occupations of the nearest-neighbor sites by the spinful Te isotopes, as shown in Fig. 8. The peaks at $T_2^* \approx 7$ μs, 10 μs, and 12 μs correspond, respectively, to the four nearest-neighbor Te sites being occupied by two ^{123}Te, one ^{123}Te, and one ^{125}Te. The possibility for more than two nearest-neighbor Te sites to be occupied by spinful Te isotopes is too small to be observed. The peaks at $T_2^* > 20$ μs correspond to none of the nearest-neighbor Te sites being occupied by spinful Te isotopes.

In addition to the surrounding Te nuclei, the Mn electron spin is also coupled to the on-site ^{55}Mn nuclear spin $I = 5/2$ through the contact hyperfine interaction $A\hat{\mathbf{M}} \cdot \hat{\mathbf{I}}$ of strength $A = 0.68\mu$eV ≈ 1 ns^{-1}. This interaction can significantly change the dynamics of the Mn electron spin on a time scale of 1 ns^{-1}. Fortunately, the ^{55}Mn nuclear spin is a well-isolated quantum system, so it does not induce irreversible Mn spin dephasing, but just modulates the Larmor precession of the Mn spin, as observed in a recent experiment by Goryca *et al.* [38]. This suggests that the ^{55}Mn nuclear spin could be utilized as a quantum memory to store long-lived quantum information.

Finally, we notice that for the electron spin qubit in semiconductor QDs, phosphorus and bismuth donors in silicon, and nitrogen-vacancy centers in diamond, the inhomogeneous dephasing caused by the static thermal fluctuation of the nuclear spin environment can be efficiently removed by spin echo techniques. Here we expect that the same technique can be used to remove the Mn spin inhomogeneous dephasing by the nuclear spin environment.

V. CONCLUSIONS

We have provided exact analytical solutions and further perform numerical simulations to study the time scale and temporal profile of the pure dephasing of a single Mn spin due to its *sp-d* exchange interaction with a fluctuating electronic environment and its hyperfine interaction with the nuclear spin environment. Our analytical results provide a clear physical picture and can be applied to estimate the Mn spin pure dephasing caused by a large variety of fluctuations of the electronic environment, such as thermal fluctuation, optical pumping, electron/hole tunneling, and electron/hole spin relaxation. It also reveals a series of interesting behaviors, such as thermal, optical, and electrical control of the crossover between the Markov and non-Markov regimes. In particular, we find that the fluctuation of the electron or hole between different orbitals due to thermal excitation or optical pumping could rapidly dephase the Mn spin on a nanosecond time scale, but this efficient pure dephasing mechanism can be strongly suppressed by applying an external electric field to tune the relative position between the Mn spin and the electron envelope functions. In the nuclear spin environment, the Mn spin inhomogeneous dephasing time is sensitive to the distribution of spinful isotopes on the nearest-neighbor lattice sites surrounding the substitutional Mn atom, with a typical inhomogeneous dephasing time of few microseconds. Our work may be useful to understanding and suppressing the Mn spin pure dephasing for its applications in quantum technologies.

ACKNOWLEDGMENTS

This work was supported by NSFC Grants No. 11274036 and No. 11322542, MOST Grant No. 2014CB848700, and the NSFC program for "Scientific Research Center" (Grant No. U1530401). We acknowledge computational support from the Beijing Computational Science Research Center (CSRC).

D.L. and W.L. contributed equally to this work.

APPENDIX A: ELECTRON–ACOUSTIC PHONON INTERACTION

Here we give a brief introduction to the calculation of acoustic phonon modes and their deformation and piezoelectric interactions with the electron.

1. Continuous elastic model

In the continuous elastic model, the displacement of the atoms is characterized by the displacement field $\mathbf{u}(\mathbf{r},t)$ obeying the equation of motion $\rho\ddot{\mathbf{u}}(\mathbf{r},t) = \nabla\cdot\boldsymbol{\sigma}$, where $\boldsymbol{\sigma}(\mathbf{r})$ is the symmetric stress tensor as determined by the symmetric strain tensor $e_{ij} = (1/2)(\partial_j u_i + \partial_i u_j)$ via $\sigma_{ij} = \sum_{kl} C_{ij,kl} e_{kl}$. In general, the elastic moduli $\boldsymbol{C}$ obey $C_{ij,kl} = C_{ji,kl} = C_{ij,lk} = C_{kl,ij}$. For a zinc-blende crystal and in the coordinate system of the crystal structure, i.e., the x direction along (100), y along (010), and z along (001), the nonvanishing elements of the elastic moduli are

$$\begin{aligned} C_{xx,xx} &= C_{yy,yy} = C_{zz,zz} \equiv C_{11},\\ C_{xx,yy} &= C_{xx,zz} = C_{yy,zz} \equiv C_{12},\\ C_{xy,xy} &= C_{xz,xz} = C_{yz,yz} = 2C_{44}, \end{aligned}$$

so the equation of motion of the displacement field reduces to

$$\begin{aligned} \rho\ddot{u}_\alpha = {} & C_{44}\nabla^2 u_\alpha + (C_{12}+C_{44})\partial_\alpha(\nabla\cdot\mathbf{u})\\ & + (C_{11}-C_{12}-2C_{44})\partial_\alpha^2 u_\alpha, \end{aligned}$$

where $\partial_\alpha \equiv \partial/\partial x_\alpha$, $\alpha = x,y,z$, and ρ is the mass density of the material. Assuming $\mathbf{u}(\mathbf{r},t) = \mathbf{e}_\mathbf{q} e^{i(\mathbf{q}\cdot\mathbf{r}-\omega t)}$, we have

$$\begin{aligned} \omega^2\rho e_{\mathbf{q}\alpha} = {} & C_{44}q^2 e_{\mathbf{q}\alpha} + (C_{12}+C_{44})q_\alpha(\mathbf{q}\cdot\mathbf{e}_\mathbf{q})\\ & + (C_{11}-C_{12}-2C_{44})q_\alpha^2 e_{\mathbf{q}\alpha}. \end{aligned}$$

For a given wave vector $\mathbf{q}$, there are three solutions, corresponding to the three acoustic branches of the phonon. For $\mathbf{q}$ along certain high-symmetric axes, the three solutions can be classified into one longitudinal acoustic (LA) mode and two transverse acoustic (TA) modes. For example, for $\mathbf{q}$ along the z axis, we have one LA mode and two degenerate TA modes with polarization vectors $\mathbf{e}_{\mathbf{q},\mathrm{LA}} = \mathbf{q}/q$ and $\mathbf{e}_{\mathbf{q},\mathrm{TA1}}, \mathbf{e}_{\mathbf{q},\mathrm{TA2}} \perp \mathbf{e}_z$ and frequencies $\omega_{\mathbf{q},\mathrm{LA}} = \sqrt{C_{11}/\rho}q$ and $\omega_{\mathbf{q},\mathrm{TA}} = \sqrt{C_{44}/\rho}q$, where $q \equiv |\mathbf{q}|$. When $\mathbf{q} = (q/\sqrt{3})(1,1,1)$, we have one LA mode and two degenerate TA modes with polarization vectors $\mathbf{e}_{\mathbf{q},\mathrm{LA}} = \mathbf{q}/q$ and $\mathbf{e}_{\mathbf{q},\mathrm{TA1}}, \mathbf{e}_{\mathbf{q},\mathrm{TA2}} \perp \mathbf{q}$, and frequencies

$$\begin{aligned} \omega_{\mathbf{q},\mathrm{LA}} &= \sqrt{(C_{11}+2C_{12}+4C_{44})/(3\rho)}q,\\ \omega_{\mathbf{q},\mathrm{TA}} &= \sqrt{(C_{11}-C_{12}+C_{44})/(3\rho)}q. \end{aligned}$$

For a general wave vector, the solutions cannot be classified into LA and TA modes. However, if we neglect the anisotropy of the solid by setting $C_{11} = C_{12} + 2C_{44}$, then the solutions always consist of one LA mode $\mathbf{e}_{\mathbf{q},\mathrm{LA}} = \mathbf{q}/q$, $\omega_{\mathbf{q},\mathrm{LA}} = \sqrt{C_{11}/\rho}q \equiv c_{\mathrm{LA}}q$ and two degenerate TA modes $\mathbf{e}_{\mathbf{q},\mathrm{TA1}}, \mathbf{e}_{\mathbf{q},\mathrm{TA2}} \perp \mathbf{q}$ and $\omega_{\mathbf{q},\mathrm{TA}} = \sqrt{C_{44}/\rho}q \equiv c_{\mathrm{TA}}q$, where c_{LA} and c_{TA} are the corresponding sound velocities.

Upon second quantization, the displacement field operator in the Schrödinger picture can be expanded as the sum of phonon modes as

$$\hat{\mathbf{u}}(\mathbf{r}) = -i\sum_{\mathbf{q}\lambda}\frac{\mathbf{e}_{\mathbf{q}\lambda}}{\sqrt{2\rho V c_\lambda q}}(\hat{a}_{\mathbf{q}\lambda} + \hat{a}^\dagger_{-\mathbf{q},\lambda})e^{i\mathbf{q}\cdot\mathbf{r}},$$

where λ runs over one LA mode and two TA modes and the polarization vectors obey the phase convention $\mathbf{e}^*_{\mathbf{q},\lambda} = -\mathbf{e}_{-\mathbf{q},\lambda}$, so that $\hat{\mathbf{u}}(\mathbf{r})$ is Hermitian. Similarly, the strain tensor can also be expanded as

$$e_{ij}(\mathbf{r}) = \frac{1}{2}\sum_{\mathbf{q}\lambda}\frac{(\mathbf{e}_{\mathbf{q}\lambda})_i q_j + (\mathbf{e}_{\mathbf{q}\lambda})_j q_i}{\sqrt{2\rho V c_\lambda q}}(\hat{a}_{\mathbf{q}\lambda} + \hat{a}^\dagger_{-\mathbf{q},\lambda})e^{i\mathbf{q}\cdot\mathbf{r}}.$$

2. Interaction between electron and acoustic phonons

There are two kinds of interactions between the electron and the acoustic phonons: the deformation potential interaction and the piezoelectric interaction. The deformation potential interaction is one of the most common phonon scattering mechanisms, in which a long-wavelength acoustic wave locally deforms the crystal and hence locally perturbs the energy bands of the electron by an amount

$$\hat{V}^{\mathrm{DP}}(\mathbf{r}) = \sum_{\alpha\beta}\Xi_{\alpha\beta}e_{\alpha\beta} \longrightarrow \Xi\nabla\cdot\mathbf{u}(\mathbf{r}),$$

where $\Xi_{\alpha\beta}$ are deformation potential constants for a particular electron energy band and the last step applies to a spherically symmetric energy band in a zinc-blende crystal, in which $\Xi_{\alpha\beta} = \delta_{\alpha\beta}\Xi$. Thus the deformation potential interaction can be written as $\hat{V}^{\mathrm{DP}}(\mathbf{r}) = \sum_{\mathbf{q}\lambda} M^{\mathrm{DP}}_{\mathbf{q}\lambda}(\hat{a}_{\mathbf{q}\lambda} + \hat{a}^\dagger_{-\mathbf{q},\lambda})e^{i\mathbf{q}\cdot\mathbf{r}}$, where

$$M^{\mathrm{DP}}_{\mathbf{q}\lambda} = \frac{\Xi(\mathbf{q}\cdot\mathbf{e}_{\mathbf{q}\lambda})}{\sqrt{2\rho V c_\lambda q}}.$$

The piezoelectric electron-phonon interaction arises from the polar nature of compound materials, such as GaAs and other III–V compounds that lack an inversion symmetry. In these materials, strain in the lattice will produce a macroscopic polarization $P_i(\mathbf{r}) = \sum_{jk} h_{ijk}e_{jk}(\mathbf{r})$ through the piezoelectric effect, where $\boldsymbol{h}$ is the piezoelectric tensor. This in turn induces a built-in electric field $\mathbf{E}(\mathbf{r}) = -\nabla\Phi(\mathbf{r})$ that can be determined from $\nabla\cdot\mathbf{D} = 0$, where $D_i(\mathbf{r}) = \sum_j \kappa_{ij}E_j(\mathbf{r}) + P_i(\mathbf{r})$ is the electric displacement vector and $\boldsymbol{\kappa}$ is the dielectric tensor. The resulting piezoelectric interaction is $V^{\mathrm{PZ}}(\mathbf{r}) = -e\Phi(\mathbf{r}) = \sum_\mathbf{q} V^{\mathrm{PZ}}_\mathbf{q} e^{i\mathbf{q}\cdot\mathbf{r}}$, where

$$V^{\mathrm{PZ}}_\mathbf{q} = ie\frac{\sum_{ijk} q_i h_{ijk} e_{jk}(\mathbf{q})}{\sum_{ij} q_i \kappa_{ij} q_j},$$

$e > 0$ is the proton charge, and $e_{ij}(\mathbf{q})$ is the Fourier transform of $e_{ij}(\mathbf{r})$. For zinc-blende crystals, we have $\kappa_{ij} = \delta_{ij}\kappa$ and the nonvanishing elements of the piezoelectric tensor are $h_{xyz} = h_{xzy} = h_{yzx} = h_{yxz} = h_{zxy} = h_{zyx} \equiv h_{14}$, so the piezoelectric interaction simplifies to $V^{\mathrm{PZ}}(\mathbf{r}) = \sum_{\mathbf{q}\lambda} M^{\mathrm{PZ}}_{\mathbf{q}\lambda}(\hat{a}_{\mathbf{q}\lambda} + \hat{a}^\dagger_{-\mathbf{q},\lambda})e^{i\mathbf{q}\cdot\mathbf{r}}$, where

$$M^{\mathrm{PZ}}_{\mathbf{q}\lambda} \equiv i\frac{eh_{14}}{\kappa\sqrt{2\rho V c_\lambda q}}A_\lambda(\theta,\varphi)$$

and

$$A_\lambda(\theta,\varphi) \equiv 2\frac{q_x q_y (\mathbf{e}_{\mathbf{q}\lambda})_z + q_y q_z (\mathbf{e}_{\mathbf{q}\lambda})_x + q_z q_x (\mathbf{e}_{\mathbf{q}\lambda})_y}{q^2}$$

is the anisotropy factor that depends on the polar angle θ and azimuth angle φ of the wave vector $\mathbf{q}$.

In zinc-blende crystals with the anisotropy neglected by setting $C_{11} = C_{12} + 2C_{44}$, the acoustic phonons can always be classified into one LA mode and two TA modes. Their polarization vectors are $\mathbf{e}_{\mathbf{q},\mathrm{LA}} = \mathbf{q}/q$, $\mathbf{e}_{\mathbf{q},\mathrm{TA1}} = (\sin\varphi, -\cos\varphi, 0)$, and $\mathbf{e}_{\mathbf{q},\mathrm{TA2}} = (\cos\theta\cos\varphi, \cos\theta\sin\varphi, -\sin\theta)$. Substituting them into the expressions of $M^{\mathrm{DP}}_{\mathbf{q}\lambda}$ and $M^{\mathrm{PZ}}_{\mathbf{q}\lambda}$ shows that only the LA mode contributes to the deformation potential interaction, while all the acoustic modes contribute to the piezoelectric interaction, with the anisotropy factor given by

$$A_{\mathrm{LA}}(\theta,\varphi) = 3\sin^2\theta\cos\theta\sin(2\varphi),$$
$$A_{\mathrm{TA1}}(\theta,\varphi) = -\sin(2\theta)\cos(2\varphi),$$
$$A_{\mathrm{TA2}}(\theta,\varphi) = \sin\theta(3\cos^2\theta - 1)\sin(2\varphi).$$

For LA phonons, the total coupling is $M_{\mathbf{q},\mathrm{LA}} = M^{\mathrm{DP}}_{\mathbf{q},\mathrm{LA}} + M^{\mathrm{PZ}}_{\mathbf{q},\mathrm{LA}}$. Since $M^{\mathrm{DP}}_{\mathbf{q},\mathrm{LA}}$ and $M^{\mathrm{PZ}}_{\mathbf{q},\mathrm{LA}}$ differ by a phase factor i, their contributions are additive:

$$\left|M_{\mathbf{q},\mathrm{LA}}\right|^2 = \left|M^{\mathrm{DP}}_{\mathbf{q},\mathrm{LA}}\right|^2 + \left|M^{\mathrm{PZ}}_{\mathbf{q},\mathrm{LA}}\right|^2.$$

APPENDIX B: NUMERICAL SOLUTION TO LINDBLAD MASTER EQUATION

In order to solve the Lindblad master equation

$$\dot{\varrho} = -i[\hat{H},\hat{\varrho}] + \sum_{\alpha}\gamma_{\alpha}\mathcal{D}[\hat{L}_{\alpha}]\hat{\varrho} \tag{B1}$$

for the density matrix $\hat{\varrho}(t)$ of the electron-Mn coupled system, we span the Hilbert space of the coupled system with the basis $|i\rangle|u\rangle|m\rangle$, with $i = 1,2$ for the electron orbitals, $u = \uparrow,\downarrow$ for the electron spin states, and $m = \pm 1/2, \pm 3/2, \pm 5/2$ for the Mn spin Zeeman eigenstates under the external magnetic field. The total number of basis states is $N = 24$, so Eq. (B1) is a set of linear equations for the $N \times N$ matrix elements $\{\varrho_{ij}\}(i,j = 1,2,\ldots,N)$:

$$\dot{\varrho}_{ij}(t) = \sum_{kl} S_{ij,kl}\varrho_{kl}(t), \tag{B2}$$

where

$$S_{ij,kl} \equiv -i(H_{ik}\delta_{j,l} - \delta_{k,i}H_{lj}) + \sum_{\alpha}\gamma_{\alpha}\left((L_{\alpha})_{ik}(L^{\dagger}_{\alpha})_{lj} - \frac{(L^{\dagger}_{\alpha}L_{\alpha})_{ik}\delta_{l,j} + \delta_{i,k}(L^{\dagger}_{\alpha}L_{\alpha})_{lj}}{2}\right),$$

and $O_{ij} \equiv \langle i|\hat{O}|j\rangle$. To solve this equation numerically, we map the N^2 matrix elements $\{\varrho_{ij}\}$ to an N^2-dimensional column vector $\mathbf{X}$, so that Eq. (B2) can be written as $\dot{\mathbf{X}} = \mathbf{S}\mathbf{X}$, where $\mathbf{S}$ is a $N^2 \times N^2$ complex matrix constructed from $\{S_{ij,kl}\}$. The solution is given by $\mathbf{X}(t) = e^{\mathbf{S}t}\mathbf{X}(0)$ and $e^{\mathbf{S}t}$ is numerically evaluated by diagonalizing the matrix $\mathbf{S}$.

[1] P. M. Koenraad and M. E. Flatte, Nat. Mater. **10**, 91 (2011).
[2] D. D. Awschalom, L. C. Bassett, A. S. Dzurak, E. L. Hu, and J. R. Petta, Science **339**, 1174 (2013).
[3] J. Fernandez Rossier, Nat. Mater. **12**, 480 (2013).
[4] J. Kobak, T. Smolenski, M. Goryca, M. Papaj, K. Gietka, A. Bogucki, M. Koperski, J.-G. Rousset, J. Suffczynski, E. Janik, M. Nawrocki, A. Golnik, P. Kossacki, and W. Pacuski, Nat. Commun. **5**, 3191 (2014).
[5] G. D. Mahan, *Many-Particle Physics* (Kluwer Academic/Plenum Publishers, New York, 2000).
[6] A. K. Bhattacharjee and J. Pérez-Conde, Phys. Rev. B **68**, 045303 (2003).
[7] F. Qu and P. Hawrylak, Phys. Rev. Lett. **95**, 217206 (2005).
[8] N. T. T. Nguyen and F. M. Peeters, Phys. Rev. B **76**, 045315 (2007).
[9] N. T. T. Nguyen and F. M. Peeters, Phys. Rev. B **78**, 245311 (2008).
[10] N. T. T. Nguyen and F. M. Peeters, Phys. Rev. B **80**, 115335 (2009).
[11] F. Qu and P. Vasilopoulos, Phys. Rev. B **74**, 245308 (2006).
[12] J. Fernández-Rossier and R. Aguado, Phys. Rev. Lett. **98**, 106805 (2007).
[13] E. Vernek, F. Qu, F. M. Souza, J. C. Egues, and E. V. Anda, Phys. Rev. B **83**, 205422 (2011).
[14] J. Fernández-Rossier and L. Brey, Phys. Rev. Lett. **93**, 117201 (2004).
[15] A. O. Govorov, Phys. Rev. B **72**, 075358 (2005).
[16] F. Qu and P. Hawrylak, Phys. Rev. Lett. **96**, 157201 (2006).
[17] A. O. Govorov, Phys. Rev. B **72**, 075359 (2005).
[18] N. T. T. Nguyen and F. M. Peeters, Phys. Rev. B **78**, 045321 (2008).
[19] I. Savic and N. Vukmirović, Phys. Rev. B **76**, 245307 (2007).
[20] W. Yang and K. Chang, Phys. Rev. B **72**, 075303 (2005).
[21] D. Hoffman, B. Meyer, A. Ekimov, I. Merkulov, A. Efros, M. Rosen, G. Couino, T. Gacoin, and J. Boilot, Solid State Commun. **114**, 547 (2000).
[22] L. Besombes, Y. Léger, L. Maingault, D. Ferrand, H. Mariette, and J. Cibert, Phys. Rev. Lett. **93**, 207403 (2004).
[23] Y. Léger, L. Besombes, L. Maingault, D. Ferrand, and H. Mariette, Phys. Rev. Lett. **95**, 047403 (2005).
[24] L. Besombes, Y. Leger, L. Maingault, D. Ferrand, H. Mariette, and J. Cibert, Phys. Rev. B **71**, 161307 (2005).
[25] Y. Léger, L. Besombes, L. Maingault, D. Ferrand, and H. Mariette, Phys. Rev. B **72**, 241309 (2005).
[26] Y. Léger, L. Besombes, L. Maingault, and H. Mariette, Phys. Rev. B **76**, 045331 (2007).
[27] J. Fernández-Rossier, Phys. Rev. B **73**, 045301 (2006).
[28] A. Kudelski, A. Lemaître, A. Miard, P. Voisin, T. C. M. Graham, R. J. Warburton, and O. Krebs, Phys. Rev. Lett. **99**, 247209 (2007).
[29] M. Goryca, P. Plochocka, T. Kazimierczuk, P. Wojnar, G. Karczewski, J. A. Gaj, M. Potemski, and P. Kossacki, Phys. Rev. B **82**, 165323 (2010).
[30] A. O. Govorov and A. V. Kalameitsev, Phys. Rev. B **71**, 035338 (2005).

[31] D. E. Reiter, T. Kuhn, and V. M. Axt, Phys. Rev. Lett. **102**, 177403 (2009).
[32] Y. Léger, L. Besombes, J. Fernández-Rossier, L. Maingault, and H. Mariette, Phys. Rev. Lett. **97**, 107401 (2006).
[33] L. Besombes, Y. Leger, J. Bernos, H. Boukari, H. Mariette, J. P. Poizat, T. Clement, J. Fernández-Rossier, and R. Aguado, Phys. Rev. B **78**, 125324 (2008).
[34] M. Goryca, T. Kazimierczuk, M. Nawrocki, A. Golnik, J. A. Gaj, P. Kossacki, P. Wojnar, and G. Karczewski, Phys. Rev. Lett. **103**, 087401 (2009).
[35] C. L. Gall, L. Besombes, H. Boukari, R. Kolodka, J. Cibert, and H. Mariette, Phys. Rev. Lett. **102**, 127402 (2009).
[36] C. L. Gall, R. S. Kolodka, C. L. Cao, H. Boukari, H. Mariette, J. Fernández-Rossier, and L. Besombes, Phys. Rev. B **81**, 245315 (2010).
[37] C. L. Gall, A. Brunetti, H. Boukari, and L. Besombes, Phys. Rev. Lett. **107**, 057401 (2011).
[38] M. Goryca, M. Koperski, P. Wojnar, T. Smoleński, T. Kazimierczuk, A. Golnik, and P. Kossacki, Phys. Rev. Lett. **113**, 227202 (2014).
[39] R. Hanson, L. P. Kouwenhoven, J. R. Petta, S. Tarucha, and L. M. K. Vandersypen, Rev. Mod. Phys. **79**, 1217 (2007).
[40] R.-B. Liu, W. Yao, and L. J. Sham, New J. Phys. **9**, 226 (2007).
[41] R.-B. Liu, W. Yao, and L. J. Sham, Adv. Phys. **59**, 703 (2010).
[42] W. Yang, W.-L. Ma, and R.-B. Liu, Rep. Prog. Phys. **80**, 016001 (2017).
[43] T. Dietl, P. Peyla, W. Grieshaber, and Y. Merle d'Aubigné, Phys. Rev. Lett. **74**, 474 (1995).
[44] C. L. Cao, L. Besombes, and J. Fernández-Rossier, Phys. Rev. B **84**, 205305 (2011).
[45] M. Goryca, M. Koperski, T. Smoleński, L. Cywiński, P. Wojnar, P. Plochocka, M. Potemski, and P. Kossacki, Phys. Rev. B **92**, 045412 (2015).
[46] M. D. Petrovic and N. Vukmirovic, Phys. Rev. B **85**, 195311 (2012).
[47] L. Cywinski, Phys. Rev. B **82**, 075321 (2010).
[48] S. Bertaina, L. Chen, N. Groll, J. Van Tol, N. S. Dalal, and I. Chiorescu, Phys. Rev. Lett. **102**, 050501 (2009).
[49] R. E. George, J. P. Edwards, and A. Ardavan, Phys. Rev. Lett. **110**, 027601 (2013).
[50] J. K. Furdyna, J. Appl. Phys. **64**, R29 (1988).
[51] A. Abragam, *The Principles of Nuclear Magnetism* (Oxford University Press, New York, 1961).
[52] A. Khaetskii, D. Loss, and L. Glazman, Phys. Rev. B **67**, 195329 (2003).
[53] K. Chen and R.-B. Liu, Phys. Rev. A **82**, 052324 (2010).
[54] P. W. Anderson, J. Phys. Soc. Jpn. **9**, 316 (1954).
[55] A. Grodecka, P. Machnikowski, and J. Förstner, Phys. Rev. B **78**, 085302 (2008).
[56] J. Danon, Phys. Rev. B **88**, 075306 (2013).
[57] J. I. Climente, A. Bertoni, G. Goldoni, and E. Molinari, Phys. Rev. B **74**, 035313 (2006).
[58] G. Piacente and G. Q. Hai, Phys. Rev. B **75**, 125324 (2007).
[59] W. Lai, Y. Cao, and Z. Ma, J. Phys.: Condens. Matter **24**, 175301 (2012).
[60] W. Lai, C. Zhang, and Z. Ma, Front. Phys. **10**, 59 (2015).
[61] T. Fujisawa, D. G. Austing, Y. Tokura, Y. Hirayama, and S. Tarucha, Nature (London) **419**, 278 (2002).
[62] O. Verzelen, R. Ferreira, G. Bastard, S. Hameau, E. Deleporte, Y. Guldner, H. Sakaki, and T. Inoshita, Phys. B (Amsterdam, Neth.) **316-317**, 1 (2002) (Proceedings of the 10th International Conference on Phonon Scattering in Condensed Matter).
[63] E. A. Zibik, T. Grange, B. A. Carpenter, N. E. Porter, R. Ferreira, G. Bastard, D. Stehr, S. Winnerl, M. Helm, H. Y. Liu, M. S. Skolnick, and L. R. Wilson, Nat. Mater. **8**, 803 (2009).
[64] T. Smoleński, T. Kazimierczuk, M. Goryca, P. Wojnar, and P. Kossacki, Phys. Rev. B **93**, 195311 (2016).
[65] T. Smoleński, T. Kazimierczuk, M. Goryca, P. Wojnar, and P. Kossacki, Phys. Rev. B **91**, 155430 (2015).
[66] X. C. Zhang, A. Pfeuffer-Jeschke, K. Ortner, V. Hock, H. Buhmann, C. R. Becker, and G. Landwehr, Phys. Rev. B **63**, 245305 (2001).
[67] D. E. Reiter, T. Kuhn, and V. M. Axt, Phys. Rev. B **83**, 155322 (2011).
[68] B. Varghese, H. Boukari, and L. Besombes, Phys. Rev. B **90**, 115307 (2014).
[69] P. Wang and W. Yang, New J. Phys. **17**, 113041 (2015).
[70] A. Wojs and P. Hawrylak, Phys. Rev. B **51**, 10880 (1995).
[71] P. Hawrylak, Phys. Rev. B **60**, 5597 (1999).
[72] H. Mathieu, J. Allegre, A. Chatt, P. Lefebvre, and J. P. Faurie, Phys. Rev. B **38**, 7740 (1988).
[73] R. Hanson, L. H. W. van Beveren, I. T. Vink, J. M. Elzerman, W. J. M. Naber, F. H. L. Koppens, L. P. Kouwenhoven, and L. M. K. Vandersypen, Phys. Rev. Lett. **94**, 196802 (2005).
[74] D. Heiss, S. Schaeck, H. Huebl, M. Bichler, G. Abstreiter, J. J. Finley, D. V. Bulaev, and D. Loss, Phys. Rev. B **76**, 241306(R) (2007).
[75] B. D. Gerardot, D. Brunner, P. A. Dalgarno, P. Ohberg, S. Seidl, M. Kroner, K. Karrai, N. G. Stoltz, P. M. Petroff, and R. J. Warburton, Nature (London) **451**, 441 (2008).
[76] T. Flissikowski, I. A. Akimov, A. Hundt, and F. Henneberger, Phys. Rev. B **68**, 161309 (2003).
[77] S. Laurent, B. Eble, O. Krebs, A. Lemaître, B. Urbaszek, X. Marie, T. Amand, and P. Voisin, Phys. Rev. Lett. **94**, 147401 (2005).